Localization in adiabatic shear flow
via geometric theory of singular perturbations

Min-Gi Lee [§]   Theodoros Katsaounis [*†‡]   Athanasios E. Tzavaras [*†¶]

Abstract

We study localization occurring during high speed shear deformations of metals leading to the formation of shear bands. The localization instability results from the competition between Hadamard instability (caused by softening response) and the stabilizing effects of strain-rate hardening. We consider a hyperbolic-parabolic system that expresses the above mechanism and construct self-similar solutions of localizing type that arise as the outcome of the above competition. The existence of self-similar solutions is turned, via a series of transformations, into a problem of constructing a heteroclinic orbit for an induced dynamical system. The dynamical system is four dimensional but has a fast-slow structure with respect to a small parameter capturing the strength of strain-rate hardening. Geometric singular perturbation theory is applied to construct the heteroclinic orbit as a transversal intersection of two invariant manifolds in the phase space.

1   Introduction

Shear bands are narrow zones of intensely localized shear that are formed during the high speed plastic deformations of metals [31, 2, 30]. They often precede rupture and are one of the striking instances of material instability leading to failure. Considerable attention has been devoted to the problem of shear band formation in both the mechanics and the applied mathematics literature, and section 2 is devoted to a presentation of the problem and a quick derivation of the hyperbolic-parabolic system

$$
\begin{aligned}
v_t &= \left(\theta^{-\alpha}\gamma^m v_x^n\right)_x, \\
\gamma_t &= v_x, \\
\theta_t &= \theta^{-\alpha}\gamma^m (v_x)^{n+1}.
\end{aligned}
\tag{1}
$$

The system describes the plastic shearing deformation of a specimen based on conservation of momentum and energy using a model in thermoviscoplasticity:

$$
\sigma = \theta^{-\alpha}\gamma^m u^n, \qquad \text{where} \quad u := \gamma_t = v_x
\tag{2}
$$

Equation (2) is viewed as a yield stress or a plastic flow rule, with the parameters α, m and $n > 0$ describing respectively the degree of thermal softening, strain hardening and strain-rate sensistivity. We refer to section 2 for a derivation of (1) and a review of earlier work useful in understanding the localization problem and its relevance to the present study; references [2, 24, 30, 17] can be consulted for further information on the mechanical aspects of the model.

[*]Computer, Electrical and Mathematical Sciences & Engineering Division, King Abdullah University of Science and Technology (KAUST), Thuwal, Saudi Arabia.

[†]Institute of Applied and Computational Mathematics, FORTH, Heraklion, Greece

[‡]Department of Mathematics and Applied Mathematics, University of Crete, Heraklion, Greece

[§]Department of Mathematics, Kyungpook National University, Daegu, Korea

[¶]Corresponding author : athanasios.tzavaras@kaust.edu.sa

The model (1) admits a special class of time-dependent solutions describing uniform shear (see (17)) and the problem of shear band formation is initially posed as a problem of stability for the uniform shearing solutions. As these are time-dependent, it leads to analysis of non-autonomous problems and presents challenges even for linearized stability. We refer to section 2 for information on this aspect of the problem. Here, we focus on the regime of linearized instability and pose the problem of understanding the behavior in the nonlinear regime. A conjecture on the threshold of instability is offered by the asymptotic analysis in [17], devising an effective equation that changes type along a threshold from forward to backward parabolic. It leads one to expect instability when $-\alpha + m + n$ changes sign from positive to negative value.

It is expedient to reformulate the problem (1), in terms of the variables (u, γ, θ), as a parabolic system where the diffusion coefficient is controlled by ordinary differential equations

$$
\begin{aligned}
u_t &= \left(\theta^{-\alpha}\gamma^m u^n\right)_{xx}, \\
\gamma_t &= u, \\
\theta_t &= \theta^{-\alpha}\gamma^m u^{n+1}.
\end{aligned}
\tag{3}
$$

The systems (1) or (3) are considered for $x \in \mathbb{R}$, $t > 0$. The goal of this work is to construct a class of self-similar solutions for systems (1) (or (3)) of the form

$$
\begin{aligned}
\gamma(t, x) &= t^a \Gamma\left(x\, t^\lambda\right), & v(t, x) &= t^b V\left(x\, t^\lambda\right), & \theta(t, x) &= t^c \Theta\left(x\, t^\lambda\right), \\
\sigma(t, x) &= t^d \Sigma\left(x\, t^\lambda\right), & u(t, x) &= t^{a-1} U\left(x\, t^\lambda\right),
\end{aligned}
\tag{4}
$$

where $\lambda > 0$ and the parameters (α, m, n) take values in the expected instability regime $-\alpha + m + n < 0$. Usually parabolic systems (such as (3)) admit diffusing self similar solutions constant on lines $\xi = \frac{x}{t^\rho}$. By insisting on $\lambda > 0$, the solutions (4) will propagate information on lines $xt^\lambda = const$ that focus around the origin. The existence of such solutions explores the invariance of the system (1) under rescalings and we look for profiles with $U(\xi)$, $\Gamma(\xi)$, $\Theta(\xi)$ even functions and $V(\xi)$ odd function.

We further demand that these profiles are localizing. We will call a self-similar function

$$
f(t, x) = t^b F(xt^\lambda), \quad \text{with } F(-\xi) = F(\xi) \text{ and } \lambda > 0
\tag{5}
$$

localizing if it has the asymptotic behavior

$$
F(\xi) = O(\xi^p) \quad \text{as } \xi \to \infty
\tag{6}
$$

and satisfies that $p < 0$ when $b > 0$ while $p > 0$ when $b < 0$. Under this definition, when $f(t, 0)$ grows then $f(t, x)$ grows at a slower rate when $x \neq 0$, while when $f(t, 0)$ decays then $f(t, x)$ decays at a slower rate at $x \neq 0$. We will call a self-similar function with an odd-profile $F(-\xi) = -F(\xi)$ localizing when its derivative $f_x(t, x)$ has the aforementioned behavior.

Applying the *ansatz* (4) leads to the system of singular ordinary differential equations

$$
\begin{aligned}
V'(\xi) &= U(\xi), \\
\Sigma'(\xi) &= bV(\xi) + \lambda\xi U(\xi), \\
a\Gamma(\xi) + \lambda\xi\Gamma'(\xi) &= U(\xi), \\
c\Theta(\xi) + \lambda\xi\Theta'(\xi) &= \Sigma(\xi)U(\xi), \\
\Sigma(\xi) &= \Theta(\xi)^{-\alpha}\Gamma(\xi)^m U(\xi)^n, \\
\Gamma(0) = \Gamma_0 > 0, \quad U(0) = U_0 > 0, &\quad \xi \in [0, \infty).
\end{aligned}
\tag{7}
$$

This is viewed as a system of singular ordinary differential equations for $(V, \Sigma, \Gamma, \Theta)$ with U defined by inverting $(7)_5$. With the objective to compare these self-similar profiles to the fundamental solution of

the heat or porous media equation, we look for solutions so that (Γ, Θ) and U is even; in turn implying that Σ is even while V is odd (see section 3 for details). We impose

$$V(0) = U'(0) = \Gamma'(0) = \Sigma'(0) = \Theta'(0) = 0 \tag{8}$$

so that the symmetric extensions are smooth self-similar profiles. The main result of this article is the construction of profiles solving (7), (8). It turns out that the induced self-similar solutions (4) exhibit localizing in space behavior as time evolves, see sections 8 and 9.

The idea of constructing self-similar localizing solutions for problems of shear band formation is introduced in [16] for the system

$$\begin{aligned} v_t &= (e^{-\alpha\theta} v_x^n)_x \\ \theta_t &= e^{-\alpha\theta} v_x^{n+1} \end{aligned} \tag{9}$$

modeling a non-Newtonian fluid with temperature dependent viscosity. Due to special properties of (9), the construction of self-similar solutions is reduced to finding a heteroclinic orbit for a planar system of autonomous differential equations, which is achieved through phase space analysis. A second step is taken in [22] where (1) is studied for parameters $\alpha = 0$ and $m < 0$ when the system simplifies to a system of two conservation laws. The problem is reduced using geometric singular perturbation theory to the flow of a planar dynamical system in a two-dimensional invariant manifold. The present work addresses the full model (1) and due to the higher dimensionality of the problem a more elaborate version of geometric singular perturbation theory is needed.

The self-similar localizing solutions emerge as the combined outcome of Hadamard instability (that characterizes the system (1) for $n = 0$ in the regime $-\alpha + m < 0$) and the regularizing effect of momentum diffusion when $n > 0$. This feature can be clearly seen in the linearized analysis of uniform shearing solutions for the simplified model (9) which indicates that the combined effect of the two mechanisms amounts to Turing instability, see [16]. Moreover, existing linearized and nonlinear stability analyses that are available for special instances of (1) and are outlined in section 2 corroborate this point.

The article is organized as follows: Sections 3 and 4 deal with the formulation of the problem leading to (7), (8). The system (7) is singular (at $\xi = 0$) and non-autonomous and it does not fit under a general existence theory. The singularity can be resolved and (7) is desingularized using again the scale-invariance properties. Furthermore, upon introducing a series of nonlinear transformations, the construction of profiles for (7), (8) is accomplished by the construction of a heteroclinic orbit for the four-dimensional dynamical system for (p, q, r, s)

$$\begin{aligned} \dot{p} &= p\Big(\frac{1}{\lambda}(r - a) + 2 - \lambda pr - q\Big), \\ \dot{q} &= q\Big(1 - \lambda pr - q\Big) + bpr, \\ n\dot{r} &= r\Big(\frac{\alpha - m - n}{\lambda(1 + \alpha)}(r - a) + \lambda pr + q + \frac{\alpha}{\lambda}r\Big(s - \frac{1 + m + n}{1 + \alpha}\Big) + \frac{n\alpha}{\lambda(1 + \alpha)}\Big), \\ \dot{s} &= s\Big(\frac{\alpha - m - n}{\lambda(1 + \alpha)}(r - a) + \lambda pr + q - \frac{1}{\lambda}r\Big(s - \frac{1 + m + n}{1 + \alpha}\Big) - \frac{n}{\lambda(1 + \alpha)}\Big), \end{aligned} \tag{S}$$

parametrized by (λ, α, m, n). The initial conditions are transmitted to asymptotic conditions for the heteroclinic as $\eta(= \log \xi) \to -\infty$ while the behavior as $\eta \to \infty$ will capture the asymptotic behavior of the profiles.

The existence of solutions to (7), (8) is achieved in sections 3 - 7. Their construction is reduced to obtaining a heteroclinic orbit for (S) with prescribed asymptotic behavior as $\eta \to -\infty$. At the end of section 3, the reader will find an outline on how the construction of the profiles is reduced to obtaining a heteroclinic orbit for (S). The existence of a heteroclinic orbit for (S) (with prescribed asymptotic behavior) is obtained in Theorem 1 using the geometric theory of singular perturbations

[9, 10, 11, 12, 20, 21], exploiting the smallness of the parameter n. Section 7 contains the main part of the proof, motivated by the geometric arguments of [25] and adapted to the present system through somewhat cumbersome computations detailed in sections 7.2 and 7.3. The proof is based on a more elaborate argument than the simple invariant manifold argument for obtaining the corresponding result for the simplified model in [22]. In the present case, the finer structure inside the manifold is needed along with the persistence of the unstable and stable manifolds, see section 7.3.

The constructed self-similar solutions depend on two parameters (U_0, Γ_0) describing the initial nonuniformity; the rate of localization λ is determined from (U_0, Γ_0) via (48). Due to the construction necessities the rate has to obey the bound (48). The solutions (4) provide an example of instabilty resulting in localization. Their localizing behavior is investigated in section 8, see Proposition 8.1 and section 8.2. In section 9, the heteroclinic orbit is computed numerically using the standardized continuation software AUTO, [6, 7, 8], what leads to graphs of the profiles and the corresponding localizing solutions for various examples of material parameters.

To our knowledge, the localizing self-similar solutions are the first instance of depicting localizing behavior for a sufficiently broad model (1) that embodies the basic shear band formation mechanism proposed by Zener and Hollomon [31] and Clifton [2], and encompasses all the contributing factors of thermal softening, strain hardening and strain-rate hardening. They complement [27], where shear bands are induced by energy supplied via the boundary. Some of the key predictions of stress-collapse are common, but the present result has the conceptual advantage to capture the emergence of localization as the combined result of Hadamard instability with small viscosity effects. It would be very interesting to study the stability of the solutions that are constructed here; this appears a challenging problem.

A preliminary report of these results, concerning the case with no strain hardening ($m = 0$), has been presented in the Proceedings article [19].

2   Description of the shear band formation problem

The formation of shear bands [4, 31] is a phenomenon occuring during high strain-rate plastic deformations of certain steels and other metal alloys. Instead of distributing evenly across the loaded region, the shear strain concentrates in a narrow band with a concurrent elevation of the temperature in the interior of the band, [31, 4, 14]. Shear bands are often precursors to rupture and their study has attracted considerable attention including experimental works [4, 14], mechanical modeling and linearized analysis studies (*e.g.* [3, 13, 23, 30] and references therein) and nonlinear analysis investigations [5, 27, 1].

2.1   Modeling shear bands

Shear bands appear and propagate as one dimensional structures (up to interaction times), and many investigations focus on the study of one-dimensional, simple shear. A specimen located in the xy-plain undergoes shear motion in the y-direction. The motion is described by the (plastic) shear strain $\gamma(t, x)$, the strain rate $u(t, x) = \gamma_t(t, x)$, the velocity $v(t, x)$ in the shear direction, the temperature $\theta(t, x)$ and the shear stress $\sigma(t, x)$ all defined in $(t, x) \in \mathbb{R}^+ \times \mathbb{R}$. It is described by the equations

$$\begin{aligned}
\gamma_t &= v_x \\
v_t &= \sigma_x \\
\theta_t &= \kappa \theta_{xx} + \sigma v_x,
\end{aligned} \tag{10}$$

which stand respectively for the kinematic compatibility equation, the balance of momentum and the balance of energy equation. Here, the elastic effects are neglected and all strain is considered to be plastic, and a Fourier heat conduction is considered with κ the thermal diffusivity.
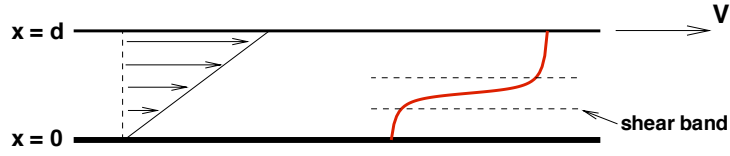
Figure 1: Uniform shear versus shear band

.

Under shearing most materials deform in a uniform fashion until they break. By contrast, in high strain-rate deformations of certain steels, it is observed that nonuniformities develop in the plastic strain and localize in a narrow region, called shear band; see Fig. 1 for a caricature of shear band forming. Shear bands correspond to material instabilities and are usually observed in the interior of specimens. Typically, the maximum temperature is measured in the interior of the band [4]. It was recognized by Zener and Hollomon [31] that the high deformation speed has two effects: First, an increase in the deformation speed changes the deformation conditions from isothermal to nearly adiabatic. Under such conditions the combined effect of thermal softening and strain hardening tends to produce net softening response. (Indeed, experimental observations of shear bands are typically associated with strain softening response – past a critical strain – of the measured stress-strain curve [3].) Second, strain rate has an effect *per se*, and needs to be included in the constitutive modeling.

Both effects are captured by modeling shear band formation via constitutive models within the framework of thermoviscoplasticity:

$$\sigma = f(\theta, \gamma, \gamma_t) \quad \text{where} \quad f_p(\theta, \gamma, p) > 0. \tag{11}$$

The constitutive relation (11) may be viewed as a yield surface or, upon inverting it, as a plastic flow rule. This suggests the terminology: the material exhibits thermal softening at state variables (θ, γ, p) where $f_\theta(\theta, \gamma, p) < 0$, strain hardening at state variables where $f_\gamma(\theta, \gamma, p) > 0$, and strain softening when $f_\gamma(\theta, \gamma, p) < 0$. The slopes of f – f_θ, f_γ or f_p – measure respectively the degree of thermal softening, strain hardening (or softening) and strain-rate sensitivity, respectively. The difficulty of performing high strain-rate experiments causes uncertainty as to the specific form of the constitutive form of the stress. Here, we will use two constitutive laws to describe the stress σ:

$$\sigma = \theta^{-\alpha} \gamma^m \gamma_t^n, \qquad \text{power law}, \tag{12}$$

$$\sigma = e^{-\alpha\theta} v_x^n, \qquad \text{exponential law}. \tag{13}$$

The power law (12) characterizes the response of the material. The parameter $\alpha > 0$ measures the degree of thermal softening, $m > 0$ measures the degree of strain hardening (or $m < 0$ in case of a softening plastic flow), while $n > 0$ measures strain-rate hardening and is typically small, $n \ll 1$, [3, 2]. It is an empirical law and the parameters are determined by fitting experimental data.

We summarize the equations describing the model. For the power law the resulting system reads

$$\begin{aligned}
v_t &= \sigma_x, \\
\theta_t &= \kappa\theta_{xx} + \sigma\gamma_t, \\
\gamma_t &= v_x, \\
\sigma &= \theta^{-\alpha}\gamma^m\gamma_t^n.
\end{aligned} \tag{14}$$

The system (14) captures the simplest mechanism proposed for shear localization in high-speed deformations of metals [31, 2], and an (isothermal) variant appears in early studies of necking [15]. Very often attention is restricted to the adiabatic model $\kappa = 0$ which is appropriate for the initial development of shear bands under very fast deformations.

The exponential law does not exhibit any strain hardening and thus (10) decouples and leads to the simplified system

$$
\begin{aligned}
v_t &= \sigma_x, \\
\theta_t &= \kappa\theta_{xx} + \sigma v_x \\
\sigma &= e^{-\alpha\theta}v_x^n .
\end{aligned}
\tag{15}
$$

The exponential law can be interpreted as a temperature dependent non-Newtonian fluid and is exactly (9) for adiabatic deformations ($\kappa = 0$).

2.2 Uniform shearing solutions

In the study of shear bands, a special problem is often considered where an infinite slab of material is sheared by prescribed constant velocity $V = 1$ at the upper plate while the lower plate is held fixed. This is described by setting the plates at $x = 0, 1$ and imposing prescribed (normalized) velocities $v(t,0) = 0$, $v(t,1) = 1$, respectively. The plates are thermally insulated: $\theta_x(t,0) = 0$, $\theta_x(t,1) = 0$. For the heat flux Q one either uses the adiabatic assumption $Q = 0$ (equivalently $\kappa = 0$) or alternatively a Fourier law, $Q = \kappa\theta_x$ with thermal diffusivity parameter κ. Imposing adiabatic conditions projects the belief that, at high strain rates, heat diffusion operates at a slower time scale than the time-scale of the development of a shear band. It appears a plausible assumption for the shear band initiation process, but not necessarily for the evolution of a developed band, due to the high temperature differences involved.

The model (14) admits a special class of solutions describing uniform shearing: They emanate from spatially uniform initial data γ_0 and θ_0, and are obtained by the *ansatz* $\gamma_s(t) = t + \gamma_0$ and $v_s(x) = x$ for the strain and velocity respectively. They are obtained upon solving the ordinary differential equation

$$
\frac{d\theta_s}{dt} = \sigma_s = \theta_s^{-\alpha}(t + \gamma_0)^m , \quad \theta_s(0) = \theta_0 ,
\tag{16}
$$

and read

$$
\begin{aligned}
&v_s(x) = x , \quad \gamma_s(t) = t + \gamma_0, \\
&\theta_s(t) = \left(\tfrac{1+\alpha}{1+m}\right)^{\frac{1}{1+\alpha}} (t+\gamma_0)^{\frac{1+m}{1+\alpha}} \left(1 + \tfrac{1+m}{1+\alpha}\big(\theta_0^{1+\alpha} - \tfrac{1+\alpha}{1+m}\gamma_0^{1+m}\big)\tfrac{1}{(t+\gamma_0)^{m+1}}\right)^{\frac{1}{1+\alpha}} \\
&\sigma_s(t) = \left(\tfrac{1+\alpha}{1+m}\right)^{-\frac{\alpha}{1+\alpha}} (t+\gamma_0)^{\frac{-\alpha+m}{1+\alpha}} \left(1 + \tfrac{1+m}{1+\alpha}\big(\theta_0^{1+\alpha} - \tfrac{1+\alpha}{1+m}\gamma_0^{1+m}\big)\tfrac{1}{(t+\gamma_0)^{m+1}}\right)^{\frac{-\alpha}{1+\alpha}} .
\end{aligned}
\tag{17}
$$

Equation $(17)_3$ describes the stress-strain curve σ_s versus γ_s for uniform shear. The stress-strain curve is increasing when $\alpha < m$ but it is decreasing for large times when $\alpha > m$. Here, we are interested in the regime $\alpha > m$ where thermal softening dominates strain hardening and produces net softening.

2.3 On the stability of the uniform shearing solution

The system (1) for $n = 0$ is a first-order system. When $\alpha > m$, the initial value problem has two purely imaginary eigenvalues in a regime of strain beyond the maximum of the stress-strain curve (see Appendix A). Accordingly, the linearized system (for $n = 0$) around the uniform shearing solution (17) exhibits *Hadamard instability*, see Appendix A.

The stability of the uniform shear solution for $n > 0$ has been the objective of many investigations. Since (17) is time dependent this leads to investigations of non-autonomous systems. A natural way to define stability is to consider

$$
\gamma_s^*(t) = t + \gamma_0, \quad \theta_s^*(t) = \left(\tfrac{1+\alpha}{1+m}\right)^{\frac{1}{1+\alpha}} (t+\gamma_0)^{\frac{1+m}{1+\alpha}} ,
\tag{18}
$$

the functions capturing the growth of the uniform shearing solution, and to study the relative perturbations

$$u(t,x) = v_x(t,x), \quad \hat{\Gamma}(t,x) = \frac{\gamma(t,x)}{\gamma_s^*(t)}, \quad \hat{\Theta}(t,x) = \frac{\theta(t,x)}{\theta_s^*(t)}. \tag{19}$$

- The uniform shear solution is *asymptotically stable* when the solution emanating from small perturbations of (17) satisfies that $(u, \hat{\Gamma}, \hat{\Theta}) \to (1,1,1)$ as time goes to infinity.

- The uniform shear solution is *unstable* if for small perturbations of (17) the relative perturbations $(u, \hat{\Gamma}, \hat{\Theta})$ drift away from $(1,1,1)$ as time increases.

This notion of stability is used in nonlinear stability studies of shear bands [5, 26] as well as in linearized stability analyses by Molinari and Clifton [23, 13] who coined the name *stability analysis of relative perturbations*. The problem of stability is presently resolved only for the special cases $m = 0$ or $\alpha = 0$ for (1); these are cases that the system decouples and reduces to simpler models:

(i) Case $m = 0$: The uniform shear is linearly stable when $-\alpha + n > 0$ and linearly unstable when $-\alpha + n < 0$ [23, 13]; it is nonlinearly stable in the region $-\alpha + n > 0$, [26].

(ii) Case $\alpha = 0$, $m > -1$: The uniform shear is linearly stable when $m + n > 0$ and linearly unstable when $m + n < 0$, [13, 29]; it is nonlinearly stable in the region $m + n > 0$, [28].

Understanding of the nature of the instability is offered in [16] for the model (9), which has the special property that both the nonlinear and the linearized analysis of relative perturbations is reduced to studying *autonomous systems*. In particular, linearized stability (or instability) can be accessed via analyzing Fourier modes; see [16]. For $n = 0$, the linearized stability analysis predicts exponential growth of the high frequency modes, leading to what is usually termed as *Hadamard instability*. By contrast, when $n > 0$ the linear modes are still unstable and their growth rates are increasing with frequency but they are uniformly bounded by a bound independent of the frequency. The behavior of the linearized system around the uniform shearing solution for the full system (1) is at present open; the conjecture is that it has the same structure as described above for relative perturbations of (9) when $n > 0$ is small, and it is stable past a certain threshold. This is corroborated by linearized analysis for the special case (1) with $\alpha = 0$, $m = -1$, $n < 1$, which again leads to the study of autonomous systems for relative perturbations, [18].

2.4 The nonlinear regime

In the unstable parameter regime, at the initial stage unstable modes start to grow and this process can be captured by the linearized problem. The second stage of localization lies within the realm of nonlinear analysis. The question arises how the high frequency oscillations resulting from Hadamard instability interact with the nonlinearity and the viscosity to form a coherent structure. An asymptotic criterion accounting for the nonlinear aspects of localization is derived in [17]. Based on ideas from the theory of relaxation system and the Chapman Enskog expansion, an effective equation is derived for the nonlinear dynamics (1). It predicts stability in the regime $-\alpha + m + n > 0$ and instability in the regime $-\alpha + m + n < 0$, see [17].

Insight on how coherent structures form can be offered by investigating self-similar solutions (4). It is customary in studies of parabolic systems (like (3)) to investigate diffusing self-similar solutions corresponding to the parameter selection $\lambda < 0$. By contrast, self-similar solutions with $\lambda > 0$ tend to propagate information along the lines $t^\lambda x = const.$ and thus to localize around the point $x = 0$. Self-similar localizing solutions were established in [16] for the model (9) using a phase-plane analysis for the resulting two-dimensional system. They will be pursued also here for the power law (1).

3   Self-similar solutions

We consider the system (1) (or the system (3)) in the domain $x \in \mathbb{R}$, $t > 0$ and note that both systems are invariant under a family of scaling transformations: if $(\gamma, u, v, \theta, \sigma)$ satisfy (1), with u, σ connected via (2), then for any $\lambda \in \mathbb{R}$ and $\rho > 0$ the rescaled functions $(\gamma_\rho, u_\rho, v_\rho, \theta_\rho, \sigma_\rho)$ defined by

$$
\begin{aligned}
\gamma_\rho(t,x) &= \rho^a \gamma(\rho^{-1} t, \rho^\lambda x), \qquad v_\rho(t,x) = \rho^b v(\rho^{-1} t, \rho^\lambda x), \\
\theta_\rho(t,x) &= \rho^c \theta(\rho^{-1} t, \rho^\lambda x), \qquad \sigma_\rho(t,x) = \rho^d \sigma(\rho^{-1} t, \rho^\lambda x), \\
u_\rho(t,x) &= \rho^{b+\lambda} \gamma(\rho^{-1} t, \rho^\lambda x)
\end{aligned}
\tag{20}
$$

also satisfies (1), provided

$$
\begin{aligned}
a &:= a_0 + a_1 \lambda = \frac{2 + 2\alpha - n}{D} + \frac{2(1+\alpha)}{D}\lambda, \qquad b := b_0 + b_1 \lambda = \frac{1+m}{D} + \frac{1+m+n}{D}\lambda, \\
c &:= c_0 + c_1 \lambda = \frac{2(1+m)}{D} + \frac{2(1+m+n)}{D}\lambda, \quad d := d_0 + d_1 \lambda = \frac{-2\alpha + 2m + n}{D} + \frac{2(-\alpha + m + n)}{D}\lambda,
\end{aligned}
\tag{21}
$$

and

$$
D = 1 + 2\alpha - m - n.
\tag{22}
$$

The same scaling trasformation leaves invariant solutions of (3). We note there are two independent scaling parameters in (20), ρ and λ, while the remaining parameters are determined by the relations (21), (22). Throughout this work, the material parameters (α, m, n) will be restricted to the range

$$
\begin{aligned}
\alpha &> 0 \quad \text{(thermal softening)}, \\
m &> -1 \quad \text{(strain softening/hardening)}, \\
n &> 0 \quad \text{(strain rate sensitivity)}, \\
-\alpha + m + n &< 0 \quad \text{(unstable regime)}.
\end{aligned}
\tag{23}
$$

Observe that $(23)_4$ implies that $-\alpha + m < 0$ and thus we are in the regime of net softening, where the associated hyperbolic system with $n = 0$ loses hyperbolicity, see Appendix A. Moreover, $D > 1 + \alpha > 1$ while $1 + \alpha - n > 1 + m > 0$.

Solutions of (1) or (3) that are self-similar with respect to the scaling transformation (20), (21), (22) have the form

$$
\begin{aligned}
\gamma(t,x) &= t^a \Gamma(t^\lambda x), \quad v(t,x) = t^b V(t^\lambda x), \qquad \theta(t,x) = t^c \Theta(t^\lambda x), \\
\sigma(t,x) &= t^d \Sigma(t^\lambda x), \quad u(t,x) = t^{b+\lambda} U(t^\lambda x),
\end{aligned}
\tag{24}
$$

and depend on one parameter, λ. In the sequel, we are interested in constructing solutions (24) defined in the domain $x \in \mathbb{R}$, $t > 0$ for values of the parameter $\lambda > 0$.

To motivate the role of self-similar solutions with $\lambda > 0$ and some forthcoming selections, recall that the fundamental solution of the heat equation $u_t = u_{xx}$ is of self-similar form

$$
u(t,x) = \frac{1}{\sqrt{t}} U\left(\frac{x}{\sqrt{t}}\right).
$$

Moreover, power nonlinear parabolic diffusion equations (such as the porous media) admit self-similar solutions which correspond to values $\lambda < 0$ and capture the effect of *diffusion*. We are interested here to investigate whether the couplings with the remaining equations in (3) can lead to the opposite behavior, of *localization*, and we seek existence of self-similar solutions with the parameter in the range $\lambda > 0$. Note that profiles of the form (24) with $\lambda > 0$ are constant on lines $\xi = t^\lambda x$ and are thus expected to localize in space as time evolves. In order to compare the solutions we intend to construct for $\lambda > 0$, with the

existing self-similar solutions of nonlinear parabolic equations, we seek solutions where $u(t, x)$ admits a maximum located at $x = 0$ for all times. This imposes for self-similar solutions that

$$U'(0) = 0 \qquad (25)$$

and as we will see this induces some symmetry properties to solutions.

Introducing the ansatz (24) into (1) gives a system of ordinary differential equations

$$\begin{aligned}
V' &= U \\
\Sigma' &= bV + \lambda \xi U \\
c\Theta + \lambda \xi \Theta' &= \Sigma U \\
a\Gamma + \lambda \xi \Gamma' &= U
\end{aligned} \qquad (26)$$

together with an algebraic equation,

$$\Sigma = \Theta^{-\alpha} \Gamma^m U^n , \qquad (27)$$

obtained from (2). This is viewed as a first order system for the variable $(V, \Sigma, \Theta, \Gamma)(\xi)$ with $U(\xi)$ determined by inverting (27). In principle, solutions of (26) will depend on five data inputs: the initial data $(V_0, \Sigma_0, \Theta_0, \Gamma_0)$ and the parameter λ. The system (26) is non-autonomous and singular at $\xi = 0$, what imposes compatibility conditions.

For smooth initial data, solutions of (3) either blow-up in finite time or they are as smooth as the initial data [27, Theorem 1] (in fact analytic for analytic initial data). Thus the self-similar solutions will be sought to be smooth with their maxima fixed at the origin. The latter can be always achieved due to the translation invariance of (3). Next, we discuss the conditions imposed by these requirements: The initial conditions

$$V(0) = V_0 \in \mathbb{R}, \quad \Sigma(0) = \Sigma_0 > 0, \quad \Theta(0) = \Theta_0 > 0, \quad \Gamma(0) = \Gamma_0 > 0, \quad U(0) = U_0 > 0 \qquad (28)$$

are supplemented with (25). Since the solution is smooth the singularity at $\xi = 0$ imposes two compatibility conditions on the data which together with (27) imply

$$a\Gamma_0 = U_0 , \quad c\Theta_0 = \Sigma_0 U_0 , \quad \Sigma_0 = \Theta_0^{-\alpha} \Gamma_0^m U_0^n \qquad (29)$$

with a, b, c given by (21). The condition $U'(0) = 0$ together with the smoothness of the solution yields upon differentiating (26) and (27)

$$\begin{aligned}
(a + \lambda)\Gamma'(0) &= U'(0) = 0 \\
(c + \lambda)\Theta'(0) &= \Sigma'(0)U(0) + \Sigma(0)U'(0) \\
&= -\alpha \frac{\Sigma_0 U_0}{\Theta_0} \Theta'(0) + m \frac{\Sigma_0 U_0}{\Gamma_0} \Gamma'(0).
\end{aligned} \qquad (30)$$

By (21) and (23), for $\lambda > 0$ we have $a > 0$, $c > 0$, hence

$$\Gamma'(0) = 0, \quad \Theta'(0) = 0 . \qquad (31)$$

Again by (25), (27), (26)$_2$ and $b > 0$,

$$\Sigma'(0) = 0, \quad V(0) = V_0 = 0 . \qquad (32)$$

Finally, since (26) is invariant under the change of variables

$$\xi \to -\xi, \quad V \to -V, \quad U \to U, \quad \Theta \to \Theta, \quad \Gamma \to \Gamma$$

9

it admits solutions such that U, Θ, Γ and Σ are even functions of ξ, while V is an odd function of ξ.

In summary, we proceed as follows: We first construct a solution $(V(\xi), \Sigma(\xi), \Theta(\xi), \Gamma(\xi))$ of (26) defined for $\xi \in [0, \infty)$ and set $U(\xi)$ by (27). The solution will be sought subject to the data

$$U'(0) = \Gamma'(0) = \Sigma'(0) = \Theta'(0) = 0 \tag{33}$$

$$V(0) = 0, \quad U(0) = U_0 > 0, \quad \Gamma(0) = \Gamma_0 > 0, \quad \Theta(0) = \Theta_0 > 0, \quad \Sigma(0) = \Sigma_0 > 0. \tag{34}$$

satisfying the compatibility conditions (29) for some $\lambda > 0$. It is not a-priori clear that this problem is not overdetermined and we give a detailed analysis of this point in Section 6. The constructed solution is then extended on $(-\infty, 0]$ by setting

$$V(-\xi) = -V(\xi), \quad U(-\xi) = U(\xi), \quad \Theta(-\xi) = \Theta(\xi), \quad \Gamma(-\xi) = \Gamma(\xi),$$

that is we use an odd extension for V and even extensions for U, Θ, Γ and Σ. Given the material constants (α, m, n) there are two independent parameters in the problem, which may be viewed as Γ_0, U_0 and $\lambda > 0$ subject to the constraint

$$\frac{U_0}{\Gamma_0} = \frac{2 + 2\alpha - n}{D} + \frac{2(1 + \alpha)}{D} \lambda. \tag{35}$$

The remaining constants Θ_0 and Σ_0 are determined via (29).

The profiles are constructed in the forthcoming sections 4-7. Then in section 8 we check that the profiles are *localizing* according to the definition (5)-(6) in the Introduction. This is based on the asymptotic behavior of the constructed profiles $\xi \to \infty$, established in Proposition 8.1.

Note that the uniform shearing solution is achieved as a self-similar profile for $\lambda = -\frac{1+m}{2(1+\alpha)} < 0$ and

$$\Gamma(\xi) = U(\xi) = U_0, \quad V(\xi) = U_0\xi, \quad \Theta(\xi) = \left(\frac{1+\alpha}{1+m} U_0^{1+m+n}\right)^{\frac{1}{1+\alpha}}, \quad \Sigma(\xi) = \left(\frac{1+\alpha}{1+m}\right)^{\frac{-\alpha}{1+\alpha}} U_0^{\frac{-\alpha+m+n}{1+\alpha}}.$$

The uniform shear should be contrasted to the solutions that are constructed here which exhibit localizing behavior: the growth of the strain is superlinear at the origin and the profiles of the solution (at fixed times) localize as time proceeds, see Section 8.

We give a short roadmap of how we proceed to construct the solution of (26), (33), (34) and determine its properties.

(a) In section 4 we de-singularize (26) and re-formulate it as an autonomous system, see (S).

(b) In section 5 we determine two equilibria M_0 and M_1 so that a heteroclinic orbit of (S) provides a meaningful, for the localization problem, self-similar profile.

(c) Section 6 discusses the behavior of (26) near $\xi = 0$ and what it implies for the heteroclinic orbit.

(d) Section 7 is the core of the proof: the geometric singular perturbation theory is used to construct a heteroclinic orbit joining M_0 to M_1 for system (S).

(e) In Section 8 we show that the self-similar profiles are localizing in the sense of Definition (5), (6) in the Introduction. In section 9 we outline a continuation method to compute the heteroclinic orbits via a standard package and provide numerical examples of the emerging solutions.

As an outcome of this construction, it turns out there is a two parameter family of solutions depending on the data U_0 and Γ_0 with the rate λ determined via (35). The dynamic stability of the solutions is a challenging open problem.

4 Reduction to the construction of a heteroclinic orbit

The goal of this section is to derive an equivalent system (S) to (26) that is autonomous and to turn the problem of constructing profiles for (26) to the construction of a heteroclinic orbit for (S). We employ techniques from [16] and [22]. The novelty of the present analysis lies in the higher dimensionality of the resulting system especially with regard to the construction of the heteroclinic orbit.

4.1 De-singularization

We regard (26) as a boundary-value problem in the right half-line $\xi \in [0, \infty)$ subject to the boundary conditions (33) and proceed to de-singularize it. The system (26) is itself scale invariant: Given a solution $\left(\Gamma(\xi), V(\xi), \Theta(\xi), \Sigma(\xi), U(\xi)\right)$ the rescaled function $\left(\Gamma_\rho(\xi), V_\rho(\xi), \Theta_\rho(\xi), \Sigma_\rho(\xi), U_\rho(\xi)\right)$ defined by

$$\Gamma_\rho(\xi) = \rho^{a_1}\Gamma(\rho\xi), \quad V_\rho(\xi) = \rho^{b_1}V(\rho\xi), \quad \Theta_\rho(\xi) = \rho^{c_1}\Theta(\rho\xi),$$
$$\Sigma_\rho(\xi) = \rho^{d_1}\Sigma(\rho\xi), \quad U_\rho(\xi) = \rho^{b_1+1}U(\rho\xi) = \rho^{a_1}U(\rho\xi) \tag{36}$$

is again a solution. The class of functions that remain invariant under this scaling transformation is

$$\left(\Gamma(\xi), V(\xi), \Theta(\xi), \Sigma(\xi), U(\xi)\right) = \left(A\xi^{-a_1}, B\xi^{-b_1}, C\xi^{-c_1}, D\xi^{-d_1}, E\xi^{-a_1}\right)$$

where A, B, C, D, E constants. Such a function is singular at $\xi = 0$ and fails to satisfy (33). Nevertheless, it suggests the change of variables

$$\bar{\gamma}(\xi) = \xi^{a_1}\Gamma(\xi), \quad \bar{v}(\xi) = \xi^{b_1}V(\xi), \quad \bar{\theta}(\xi) = \xi^{c_1}\Theta(\xi), \quad \bar{\sigma}(\xi) = \xi^{d_1}\Sigma(\xi), \quad \bar{u}(\xi) = \xi^{b_1+1}U(\xi), \tag{37}$$

with a_1, b_1, c_1 and d_1 as in (21), in order to de-singularize the problem. After some cumbersome, but straightforward calculation, we find that $(\bar{\gamma}, \bar{v}, \bar{\theta}, \bar{\sigma})$ satisfies

$$\begin{aligned}
a_0\bar{\gamma} + \lambda\xi\bar{\gamma}' &= \bar{u}, \\
b_0\bar{v} + \lambda\xi\bar{v}' &= -d_1\bar{\sigma} + \xi\bar{\sigma}', \\
c_0\bar{\theta} + \lambda\xi\bar{\theta}' &= \bar{\sigma}\bar{u}, \\
-b_1\bar{v} + \xi\bar{v}' &= \bar{u},
\end{aligned} \tag{38}$$

and $\bar{u}$ is defined by

$$\tilde{\sigma} = \bar{\theta}^{-\alpha}\bar{\gamma}^m\bar{u}^n.$$

Next, introduce a new independent variable $\eta = \log\xi$ and define $(\tilde{\gamma}, \tilde{v}, \tilde{\theta}, \tilde{\sigma}, \tilde{u})$ by

$$\begin{aligned}
\tilde{\gamma}(\log\xi) &= \bar{\gamma}(\xi), \quad \tilde{v}(\log\xi) = \bar{v}(\xi), \quad \tilde{\theta}(\log\xi) = \bar{\theta}(\xi), \\
\tilde{\sigma}(\log\xi) &= \bar{\sigma}(\xi), \quad \tilde{u}(\log\xi) = \bar{u}(\xi).
\end{aligned} \tag{39}$$

Noticing that $\frac{d}{d\eta}\tilde{\gamma}(\eta) = \xi\frac{d}{d\xi}\bar{\gamma}(\xi)$, we obtain an autonomous system

$$\begin{aligned}
a_0\tilde{\gamma} + \lambda\dot{\tilde{\gamma}} &= \tilde{u}, \\
b_0\tilde{v} + \lambda\dot{\tilde{v}} &= -d_1\tilde{\sigma} + \dot{\tilde{\sigma}}, \\
c_0\tilde{\theta} + \lambda\dot{\tilde{\theta}} &= \tilde{\sigma}\tilde{u}, \\
-b_1\tilde{v} + \dot{\tilde{v}} &= \tilde{u},
\end{aligned} \tag{40}$$

where the notation $\dot{f} = \frac{df}{d\eta}$ is used, and $\tilde{u}$ is defined by

$$\tilde{\sigma} = \tilde{\theta}^{-\alpha}\tilde{\gamma}^m\tilde{u}^n.$$

The system (40) is autonomous and one might attempt to consider its equilibria. However, it is easy to conclude that we cannot expect a heteroclinic that tends to equilibria of (40). Indeed, suppose $\tilde{u} \to \tilde{u}_\infty \geq 0$ as $\eta \to \infty$. Then from the last equation in (40), we conclude that $\tilde{v} \to \infty$. This suggests to enlarge the scope and consider solutions that grow as polynomials (or faster) at infinities.

4.2 The (p, q, r, s)-system derivation

Next, we attempt to come up with a new choice of variables that tend to equilibria as $\eta \to \pm\infty$ and accommodate orbits that have power behavior at infinities. We rewrite (40) in the form

$$\frac{d}{d\eta}(\ln \tilde{\gamma}) = \tfrac{1}{\lambda}\Big(-a_0 + \frac{\tilde{u}}{\tilde{\gamma}}\Big),$$
$$\frac{d}{d\eta}(\ln \tilde{v}) = b_1 + \frac{\tilde{u}}{\tilde{v}},$$
$$\frac{d}{d\eta}(\ln \tilde{\theta}) = \tfrac{1}{\lambda}\Big(-c_0 + \frac{\tilde{\sigma}\tilde{u}}{\tilde{\theta}}\Big),$$
$$\frac{d}{d\eta}(\ln \tilde{\sigma}) = d_1 + b\frac{\tilde{v}}{\tilde{\sigma}} + \lambda\frac{\tilde{u}}{\tilde{\sigma}}$$

(41)

and view it as describing the evolution of $(\tilde{\gamma}, \tilde{v}, \tilde{\theta}, \tilde{\sigma})$ with $\tilde{u}$ determined by $\tilde{u} = \big(\frac{\tilde{\sigma}}{\tilde{\theta}^{-\alpha}\tilde{\gamma}^m}\big)^{\frac{1}{n}}$.

This leads us to define

$$p := \frac{\tilde{\gamma}}{\tilde{\sigma}}, \quad q := b\frac{\tilde{v}}{\tilde{\sigma}}, \quad r = \Big(\frac{\tilde{\sigma}}{\tilde{\theta}^{-\alpha}\tilde{\gamma}^{m+n}}\Big)^{\frac{1}{n}} = \frac{\tilde{u}}{\tilde{\gamma}}, \quad s := \frac{\tilde{\sigma}\tilde{\gamma}}{\tilde{\theta}}.$$

(42)

The transformation $(p, q, r, s) \leftrightarrow (\tilde{\gamma}, \tilde{v}, \tilde{\theta}, \tilde{\sigma})$ is a bijection in the positive orthant with the inverse determined by

$$\tilde{\gamma} = p^{\frac{1+\alpha}{D}} s^{\frac{\alpha}{D}} r^{\frac{n}{D}}, \quad \tilde{\theta} = p^{\frac{1+m+n}{D}} s^{\frac{m+n-1}{D}} r^{\frac{2n}{D}},$$

and then

$$\tilde{\sigma} = \frac{1}{\tilde{\gamma}}p, \quad \tilde{v} = \frac{1}{b}\tilde{\sigma}q = \frac{1}{b}\frac{pq}{\tilde{\gamma}}.$$

Using (41) and (42), we write

$$\frac{\dot{p}}{p} = \frac{\dot{\tilde{\gamma}}}{\tilde{\gamma}} - \frac{\dot{\tilde{\sigma}}}{\tilde{\sigma}} \qquad = \Big[\tfrac{1}{\lambda}\Big(\frac{\tilde{u}}{\tilde{\gamma}} - a_0\Big)\Big] \qquad - \Big[d_1 + b\frac{\tilde{v}}{\tilde{\sigma}} + \lambda\frac{\tilde{u}}{\tilde{\gamma}}\frac{\tilde{\gamma}}{\tilde{\sigma}}\Big]$$

$$\frac{\dot{q}}{q} = \frac{\dot{\tilde{v}}}{\tilde{v}} - \frac{\dot{\tilde{\sigma}}}{\tilde{\sigma}} \qquad = \Big[b_1 + \frac{\tilde{u}}{\tilde{v}}\Big] \qquad - \Big[d_1 + b\frac{\tilde{v}}{\tilde{\sigma}} + \lambda\frac{\tilde{u}}{\tilde{\gamma}}\frac{\tilde{\gamma}}{\tilde{\sigma}}\Big]$$

$$n\frac{\dot{r}}{r} = -(m+n)\frac{\dot{\tilde{\gamma}}}{\tilde{\gamma}} + \frac{\dot{\tilde{\sigma}}}{\tilde{\sigma}} + \alpha\frac{\dot{\tilde{\theta}}}{\tilde{\theta}} \qquad = \Big[\frac{-(m+n)}{\lambda}\Big(\frac{\tilde{u}}{\tilde{\gamma}} - a_0\Big)\Big] \quad + \Big[d_1 + b\frac{\tilde{v}}{\tilde{\sigma}} + \lambda\frac{\tilde{u}}{\tilde{\gamma}}\frac{\tilde{\gamma}}{\tilde{\sigma}}\Big] + \Big[\frac{\alpha}{\lambda}\Big(\frac{\tilde{\sigma}\tilde{u}}{\tilde{\theta}} - c_0\Big)\Big]$$

$$\frac{\dot{s}}{s} = \frac{\dot{\tilde{\gamma}}}{\tilde{\gamma}} + \frac{\dot{\tilde{\sigma}}}{\tilde{\sigma}} - \frac{\dot{\tilde{\theta}}}{\tilde{\theta}} \qquad = \Big[\tfrac{1}{\lambda}\Big(\frac{\tilde{u}}{\tilde{\gamma}} - a_0\Big)\Big] \qquad + \Big[d_1 + b\frac{\tilde{v}}{\tilde{\sigma}} + \lambda\frac{\tilde{u}}{\tilde{\gamma}}\frac{\tilde{\gamma}}{\tilde{\sigma}}\Big] - \Big[\tfrac{1}{\lambda}\Big(\frac{\tilde{\sigma}\tilde{u}}{\tilde{\theta}} - c_0\Big)\Big].$$

We note that

$$\frac{\tilde{\sigma}\tilde{u}}{\tilde{\theta}} = rs, \quad \frac{\tilde{u}}{\tilde{v}} = \frac{bpr}{q}, \quad \frac{\tilde{u}}{\tilde{\sigma}} = pr,$$

and using (21) and (22), after a cumbersome but straightforward calculation, we derive the (p, q, r, s)-system:

$$\dot{p} = p\Big(\frac{1}{\lambda}(r - a) + 2 - \lambda pr - q\Big),$$
$$\dot{q} = q\Big(1 - \lambda pr - q\Big) + bpr,$$
$$n\dot{r} = r\Big(\frac{\alpha - m - n}{\lambda(1 + \alpha)}(r - a) + \lambda pr + q + \frac{\alpha}{\lambda}r\Big(s - \frac{1 + m + n}{1 + \alpha}\Big) + \frac{n\alpha}{\lambda(1 + \alpha)}\Big),$$
$$\dot{s} = s\Big(\frac{\alpha - m - n}{\lambda(1 + \alpha)}(r - a) + \lambda pr + q - \frac{1}{\lambda}r\Big(s - \frac{1 + m + n}{1 + \alpha}\Big) - \frac{n}{\lambda(1 + \alpha)}\Big).$$

(S)

12

In the sequel, we analyze (S) as an autonomous system: We begin with sorting its equilibria and analyzing their linear stability. Most importantly, (S) possesses the *fast-slow* structure because of the small parameter n in the left-hand-side of $(S)_3$; the dynamics of r can be distinctively faster than those of the other variables off the nullcline of r.

5 Equilibria and their linear stability

System (S) admits several equilibria listed in Appendix B. Our region of interest is the sector

$$\mathscr{P} = \{(p, q, r, s) \mid p \geq 0, q \geq 0, r > 0, s > 0\}.$$

That $p, q \geq 0$ comes from the requirement that $\tilde{\gamma}, \tilde{v}, \tilde{\sigma} \geq 0$. The reason we restrict to $r > 0$, $s > 0$ stems from mechanical considerations: If we transform back to the original variables, then we find

$$r(\eta)|_{\eta=t^\lambda x} = t\partial_t \log \gamma(t, x), \quad r(\eta)s(\eta)|_{\eta=t^\lambda x} = t\partial_t \log \theta(t, x).$$

Shear band initiation is related to conditions of loading where both the plastic strain and the temperature are increasing. This motivates to restrict to self-similar solutions taking values in the region $r > 0$, $s > 0$.

From the complete set of equilibria for (S) listed in Appendix B only two reside in the region $r > 0$, $s > 0$, namely

$$M_0 = (0, 0, r_0, s_0), \qquad r_0 = a, \qquad s_0 = \frac{1 + m + n}{1 + \alpha} - \frac{n}{(1 + \alpha)r_0},$$

$$M_1 = (0, 1, r_1, s_1), \qquad r_1 = a - \frac{1 + \alpha}{\alpha - m - n}\lambda, \qquad s_1 = \frac{1 + m + n}{1 + \alpha} - \frac{n}{(1 + \alpha)r_1}.$$

Here, we recall (21), (22):

$$a = a_0 + a_1\lambda = \frac{2 + 2\alpha - n}{D} + \frac{2 + 2\alpha}{D}\lambda$$

$$D = 1 + 2\alpha - m - n,$$

and that the parameters (α, m, n) take values in the range (23). As a consequence $r_0 > 0$, and a simple calculation shows that $r_0 s_0 = \frac{2(1+m)}{D} + \frac{2(1+m+n)}{D}\lambda > 0$; hence, $r_0, s_0 > 0$ and M_0 resides in the region $\mathscr{P}$. By contrast, M_1 can be out of the region $r > 0$, $s > 0$ if λ is large enough. Note that $r_1, s_1 > 0$ only if $\frac{1+m+n}{1+\alpha}r_1 > \frac{n}{(1+\alpha)}$. This reads

$$\frac{1 + m + n}{1 + \alpha}\left(\frac{2 + 2\alpha - n}{D} - \frac{(1 + \alpha)(1 + m + n)}{D(\alpha - m - n)}\lambda\right) > \frac{n}{(1 + \alpha)},$$

and thus M_1 resides in the region $\mathscr{P}$ only under the constraint

$$0 < \lambda < \frac{2(\alpha - m - n)}{1 + m + n}\left(\frac{1 + m}{1 + m + n}\right). \tag{43}$$

Henceforth, we restrict attention to rates λ satisfying (43).

We denote the four eigenvalues and four eigenvectors of the vector field linearized at M_i, $i = 0, 1$, by μ_{ij} and X_{ij} with $j = 1, 2, 3, 4$.

- M_0 is a saddle; the matrix of the linearized vector field at M_0 has three positive eigenvalues and one negative eigenvalue.

$$\mu_{01} = 2, \quad \mu_{02} = 1, \quad \mu_{03} = \mu_0^+ = O\left(\frac{1}{n}\right) > 0, \quad \mu_{04} = \mu_0^- < 0, \tag{44}$$
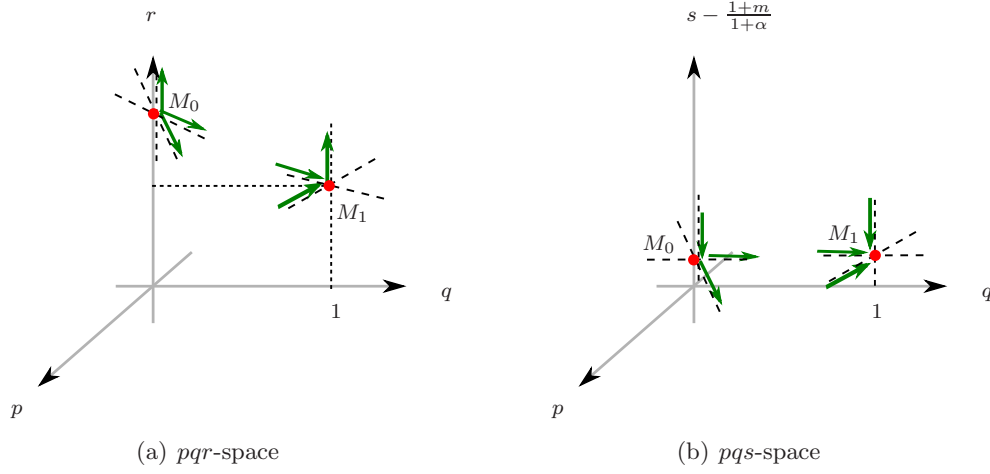
13

(a) *pqr*-space   (b) *pqs*-space

Figure 2: Eigenvectors around M_0 and M_1 in *pqr*-space and in *pqs*-space respectively ($\mu_{11} \neq -1$ and $n \ll 1$).

where $\mu_0^{\pm}$ are respectively a positive and a negative solution of the quadratic equation

$$\left(\mu - \frac{r_0}{n}\left(\frac{1-s_0}{\lambda} - \frac{n}{\lambda r_0}\right)\right)\left(\mu + \frac{s_0 r_0}{\lambda}\right) - \frac{s_0 r_0 (1-s_0)(\alpha r_0)}{n\lambda^2} = 0.$$

The leading orders of $\mu_0^{\pm}$ are given by

$$\mu_0^+ = \frac{1}{n}\frac{2(\alpha - m)(1+\alpha)(1+\lambda)}{\lambda(1+\alpha)(1+2\alpha - m)} + O(1), \quad \mu_0^- = -\frac{2(1+m)(1+\alpha)(1+\lambda)}{\lambda(1+2\alpha - m)} + O(n).$$

Notice that one of the positive eigenvalue μ_{03} is $O(\frac{1}{n})$, which indicates the separably fast dynamics along the direction X_{03}. We will make use of this structure later. The precise eigenvector components are presented in Appendix C, the directions of the eigenvectors are pointed out in Fig. 2 for n sufficiently small.

- M_1 is a saddle; the matrix of the linearized vector field at M_1 has one positive eigenvalue and three negative eigenvalues.

$$\mu_{11} = -\frac{1+m+n}{\alpha - m - n}, \quad \mu_{12} = -1, \quad \mu_{13} = \mu_1^+ = O\left(\frac{1}{n}\right) > 0, \quad \mu_{14} = \mu_1^- < 0, \tag{45}$$

where $\mu_1^{\pm}$ is respectively a positive and a negative solution of the quadratic equation

$$\left(\mu - \frac{r_1}{n}\left(\frac{1-s_1}{\lambda} - \frac{n}{\lambda r_1}\right)\right)\left(\mu + \frac{s_1 r_1}{\lambda}\right) - \frac{s_1 r_1 (1-s_1)(\alpha r_1)}{n\lambda^2} = 0.$$

The leading orders of $\mu_1^{\pm}$ are given by

$$\mu_1^+ = \frac{\alpha - m}{n\lambda(1+\alpha)}\left(\frac{2(1+\alpha)(1+\lambda)}{(1+2\alpha - m)} - \frac{1+\alpha}{\alpha - m - n}\lambda\right) + O(1),$$

$$\mu_1^- = -\frac{1+m}{\lambda}\left(\frac{2(1+\alpha)(1+\lambda)}{(1+2\alpha - m)} - \frac{1+\alpha}{\alpha - m - n}\lambda\right) + O(n).$$

Note that the positive eigenvalue μ_{13} is $O(\frac{1}{n})$. In constrast to what happens at M_0, the eigenvalues of the linearized vector field at M_1 may have multiplicity higher than one. Appendix C describes the possible cases and provides the generalized eigenvectors when necessary.

14

6 Characterization of the heteroclinic orbit

The equilibrium M_0 has a three dimensional unstable manifold and a one dimensional stable manifold while the equilibrium M_1 has a three dimensional stable manifold and a one-dimensional unstable manifold. There is one unstable direction for each equilibrium corresponding to a positive eigenvalue of order $O(\frac{1}{n})$. Due to the high dimensionality, it is difficult to read the complete behavior of the flow in phase space. This section aims to develop a picture of the flow on the positive orthant $p, q, r, s > 0$ and to associate the behavior of the system (26) near the singular point $\xi = 0$ with the behavior of the system (S) around M_0.

6.1 Behavior near the singular point $\xi = 0$

We begin with the latter point. The following proposition states how (28), (25) are transmitted to the asymptotic behavior of (p, q, r, s) around the equilibrium M_0 as $\eta \to -\infty$.

Proposition 6.1. *Let $\big(V, \Sigma, \Theta, \Gamma\big)(\xi)$ be a smooth solution of (26), $U(\xi)$ be defined by (27), and suppose the solution is defined for $\xi > 0$, is smooth, takes values in the positive orthant, and assumes the initial conditions*

$$V(0) = V_0 \geq 0, \quad \Sigma(0) = \Sigma_0 > 0, \quad \Theta(0) = \Theta_0 > 0 \quad \Gamma_0 = \Gamma_0 > 0 \quad and \ U'(0) = 0.$$

Then $\big(V, \Sigma, \Theta, \Gamma\big)$ and U satisfy at $\xi = 0$ the conditions (29), (33), (34). Morever, the orbit defined by the transformations (37), (39), (42), $\chi(\eta) = (p(\eta), q(\eta), r(\eta), s(\eta)) \to M_0$ as $\eta \to -\infty$. Furthermore, it tends to M_0 along the direction of the first eigenvector X_{01}, in fact

$$e^{-2\eta}\big(\chi(\eta) - M_0\big) \to \kappa X_{01}, \quad for \ some \ constant \ \kappa > 0 \ as \ \eta \to -\infty. \tag{46}$$

Remark 6.1. The orbit approaches M_0 tangent to X_{01} as $\eta \to -\infty$. Since M_0 has a three-dimensional unstable manifold and $\mu_{02}(= 1) < \mu_{01}(= 2) < \mu_{03}(= O(\frac{1}{n}))$, the orbits emanating from M_0 tangent to X_{01} all lie on a two dimensional manifold that at M_0 is tangent to the plane spanned by X_{01} and X_{03}. This two dimensional submanifold will be referred to as the Strongly unstable manifold of M_0.

Proof. Assuming smoothness and boundedness of $\big(V, \Sigma, \Theta, \Gamma\big)$ and U in a neighborhood of $\xi = 0$ and the conditions (25), (28) we deduce first (29), (33), (34) by the argument of section 3. The derivatives of $\big(\Gamma, V, \Theta, \Sigma, U\big)$ at $\xi = 0$ are obtained by differentiating the system (26) repeatedly. Re-write (26) as

$$a + \lambda \xi \frac{\Gamma'}{\Gamma} = \frac{U}{\Gamma}, \qquad\qquad c + \lambda \xi \frac{\Theta'}{\Theta} = \frac{\Sigma \Gamma}{\Theta} \frac{U}{\Gamma},$$

$$(b + \lambda)U + \lambda \xi U'(\xi) = \Sigma'' = \Big(\frac{\Sigma \Gamma}{\Theta} \frac{\Theta}{\Gamma}\Big)'', \qquad \frac{\big(\frac{\Sigma \Gamma}{\Theta}\big)''}{\frac{\Sigma \Gamma}{\Theta}} = (1 + m + n)\frac{\Gamma''}{\Gamma} - (1 + \alpha)\frac{\Theta''}{\Theta} + n\frac{\big(\frac{U}{\Gamma}\big)''}{\frac{U}{\Gamma}},$$

from where after a computation we conclude

$$\frac{U}{\Gamma}(0) = a = r_0, \qquad \Big(\frac{U}{\Gamma}\Big)'(0) = 0, \qquad \Big(\frac{U}{\Gamma}\Big)''(0) = \frac{\Gamma(0)}{\Sigma(0)} \frac{-2(b + \lambda)r_0}{\frac{1 - s_0}{\lambda} - \frac{n}{r_0}\Big(\frac{2}{s_0} + \frac{r_0}{\lambda}\Big)\Big(\frac{\frac{1}{\lambda} + 2}{\frac{1 + \alpha}{\lambda}r_0 + \frac{2}{s_0}}\Big)},$$

$$\frac{\Sigma \Gamma}{\Theta}(0) = \frac{c}{a} = s_0, \qquad \Big(\frac{\Sigma \Gamma}{\Theta}\Big)'(0) = 0, \qquad \Big(\frac{\Sigma \Gamma}{\Theta}\Big)''(0) = \frac{n}{r_0}\Big(\frac{\frac{1}{\lambda} + 2}{\frac{1 + \alpha}{\lambda}r_0 + \frac{2}{s_0}}\Big)\Big(\frac{U}{\Gamma}\Big)''(0).$$

15

The Taylor expansions of $p(\log \xi)$, $q(\log \xi)$, $r(\log \xi)$ and $s(\log \xi)$ at $\xi = 0$ are computed using (37), (42), (33) and the relations above,

$$p(\log \xi) = \frac{\bar{\gamma}}{\bar{\sigma}} = \frac{\xi^{a_1} \Gamma(\xi)}{\xi^{d_1} \Sigma(\xi)} = \xi^2 \frac{\Gamma(\xi)}{\Sigma(\xi)} = \xi^2 \frac{\Gamma(0)}{\Sigma(0)} + o(\xi^2),$$

$$q(\log \xi) = b \frac{\bar{v}}{\bar{\sigma}} = b \frac{\xi^{b_1} V(\xi)}{\xi^{d_1} \Sigma(\xi)} = b \xi \frac{V(\xi)}{\Sigma(\xi)} = b \xi^2 \frac{U(0)}{\Sigma(0)} + o(\xi^2) = \xi^2 \; b r_0 \frac{\Gamma(0)}{\Sigma(0)} + o(\xi^2),$$

$$r(\log \xi) = \frac{\bar{u}}{\bar{\gamma}} = \frac{\xi^{1+b_1} U(\xi)}{\xi^{a_1} \Gamma(\xi)} = \frac{U(0)}{\Gamma(0)} + \xi \left(\frac{U}{\Gamma}\right)'(0) + \frac{1}{2}\xi^2 \left(\frac{U}{\Gamma}\right)''(0) + o(\xi^2)$$

$$= \frac{U}{\Gamma}(0) + \xi^2 \frac{\Gamma(0)}{\Sigma(0)} \frac{-(b+\lambda)r_0}{\frac{1-s_0}{\lambda} - \frac{n}{r_0}\left(\frac{2}{s_0} + \frac{r_0}{\lambda}\right)\left(\frac{\frac{1}{\lambda}+2}{\frac{1+\alpha}{\lambda}r_0 + \frac{2}{s_0}}\right)},$$

$$s(\log \xi) = \frac{\bar{\sigma}\bar{\gamma}}{\bar{\theta}} = \frac{\xi^{a_1+d_1}\Sigma(\xi)\Gamma(\xi)}{\xi^{c_1}\Theta(\xi)} = \frac{\Sigma\Gamma}{\Theta}(0) + \xi\left(\frac{\Sigma\Gamma}{\Theta}\right)'(0) + \frac{1}{2}\xi^2\left(\frac{\Sigma\Gamma}{\Theta}\right)''(0) + o(\xi^2)$$

$$= \frac{\Sigma\Gamma}{\Theta}(0) + \xi^2 n \left(\frac{\left(\frac{1}{\lambda}+2\right)\frac{1}{r_0}}{\frac{1+\alpha}{\lambda}r_0 + \frac{2}{s_0}}\right) \frac{\Gamma(0)}{\Sigma(0)} \frac{-(b+\lambda)r_0}{\frac{1-s_0}{\lambda} - \frac{n}{r_0}\left(\frac{2}{s_0} + \frac{r_0}{\lambda}\right)\left(\frac{\frac{1}{\lambda}+2}{\frac{1+\alpha}{\lambda}r_0 + \frac{2}{s_0}}\right)} + o(\xi^2).$$

Therefore, taking note of the eigenvector X_{01} in Appendix C, we conclude

$$\chi(\log \xi) - M_0 = \big(p(\log \xi), q(\log \xi), r(\log \xi), s(\log \xi)\big) - M_0 = \frac{\Gamma(0)}{\Sigma(0)}\xi^2 X_{01} + o(\xi^2),$$

which implies (46) since $\eta = \log \xi \to -\infty$ as $\xi \to 0$. $\qquad\square$

Remark 6.2. For n small enough, we find that second derivatives have definite signs: $\left(\frac{U}{\Gamma}\right)''(0) < 0$, $\left(\frac{\Sigma\Gamma}{\Theta}\right)''(0) < 0$, and

$$\frac{\Gamma''(0)}{\Gamma(0)} = \frac{1}{2\lambda}\left(\frac{U}{\Gamma}\right)''(0) < 0, \qquad \frac{\Theta''(0)}{\Theta(0)} = \frac{1}{2\lambda}\left(s_0\left(\frac{U}{\Gamma}\right)''(0) + r_0\left(\frac{\Sigma\Gamma}{\Theta}\right)''(0)\right)\right) < 0,$$

$$\frac{U''(0)}{U(0)} = \frac{\Gamma''(0)}{\Gamma(0)} + \frac{\left(\frac{U}{\Gamma}\right)''(0)}{\frac{U}{\Gamma}(0)} < 0, \quad \Sigma''(0) = (b+\lambda)U(0) > 0. \tag{47}$$

6.2 A heteroclinic orbit

The behavior of (26) near the singular point $\xi = 0$ suggests to look for an orbit of (S) emanating from M_0 in the direction of the Strongly unstable manifold. At the other end point, as $\eta \to \infty$, we expect that the variables p, q, r and s equilibrate to a bounded state as $\eta \to \infty$. This would imply that the variables $\tilde{\gamma}$, $\tilde{v}$, $\tilde{\theta}$, and $\tilde{\sigma}$ grow at most exponentially in η as seen from (41) and in turn polynomially in ξ. Therefore, we look for a heteroclinic orbit joining M_0 with M_1, the only two equilibria in the sector $r > 0$ and $s > 0$. That is we expect $\chi(\eta) \to M_1$ as $\eta \to \infty$. The heteroclinic orbit will be called $\chi(\eta)$ for the rest of this paper. It will be constructed in the next section.

The two end point behaviors can be interpreted geometrically as well: The end point behavior as $\eta \to -\infty$ specifies a nontrivial submanifold of the unstable manifold of the equilibrium M_0 from which the orbit emanates. This submanifold will turn out to intersect the stable manifold of M_1 and the intersection of these two manifold is the heteroclinic orbit we search for.

U_0, Γ_0 are selected.

Given the heteroclinic $\chi(\eta)$, this subsection is devoted to adapting the initial data. By data we refer to $(\Gamma_0, \Theta_0, \Sigma_0, U_0)$.

6.3 Adapting the initial data

Suppose now that an orbit $\chi(\eta)$ has been constructed that satisfies (S), it emanates from M_0 in the Strongly unstable manifold, i.e. it satisfies (46), and connects to M_1. The orbit corresponds to a set of parameters (λ, α, m, n). We proceed to show how the data input $(V_0, \Gamma_0, \Theta_0, \Sigma_0, U_0)$ fit under the supposed orbit $\chi^{\lambda, \alpha, m, n}(\eta)$. From (34), (29) we know that $V_0 = 0$ and

$$\Theta_0 = c^{-\frac{1}{1+\alpha}} \Gamma_0^{\frac{m}{1+\alpha}} U_0^{\frac{1+n}{1+\alpha}}, \quad \Sigma_0 = c^{\frac{\alpha}{1+\alpha}} \Gamma_0^{\frac{m}{1+\alpha}} U_0^{-\frac{\alpha-n}{1+\alpha}}.$$

By (35), the rate of growth λ determines the ratio $\frac{U_0}{\Gamma_0}$

$$\lambda = \left(\frac{U_0}{\Gamma_0} - \frac{2(1+\alpha) - n}{D} \right) \frac{D}{2(1+\alpha)}. \tag{48}$$

Note finally that the restriction (43) on the growth rate λ implies a restriction on the ratio

$$\frac{2(1+\alpha) - n}{D} < \frac{U_0}{\Gamma_0} < \frac{2(1+\alpha) - n}{D} + \frac{4(1+\alpha)(\alpha - m - n)(1+m)}{D(1+m+n)^2}$$
$$= \frac{2(1+\alpha)}{1+m+n} - \frac{n}{D} \left(\frac{4(1+\alpha)(\alpha - m - n)}{(1+m+n)^2} + 1 \right). \tag{49}$$

It remains to resolve only one degree of freedom. The orbit $\chi(\eta)$ emanating from M_0 in the direction X_{01} satisfies the asymptotic expansion

$$\chi(\eta) - M_0 = \kappa_1 e^{\mu_{01}\eta} X_{01} + \kappa_3 e^{\mu_{03}\eta} X_{03} + \text{higher-order terms as } \eta \to -\infty, \tag{50}$$

for two constants κ_1 and κ_3. Any reparametrization $\chi(\eta - \eta_0)$, $\eta_0 \in \mathbb{R}$, depicts the same heteroclinic orbit. Define $\bar{\chi}(\eta) = \chi(\eta - \eta_0)$ and we proceed to select η_0 so as to satisfy the data. Then,

$$\lim_{\eta \to -\infty} \left(\bar{\chi}(\eta) - M_0 \right) e^{-2\eta} = \lim_{\eta \to -\infty} \left(\left(\chi(\eta - \eta_0) - M_0 \right) e^{-2(\eta - \eta_0)} \right) e^{-2\eta_0} = e^{-2\eta_0} \kappa_1 X_{01}.$$

On the other hand, from the proof of Proposition 6.1,

$$\lim_{\eta \to -\infty} \left(\bar{\chi}(\eta) - M_0 \right) e^{-2\eta} = \frac{\Gamma_0}{\Sigma_0} X_{01},$$

which dictates we fix the last degree of freedom by selecting

$$\eta_0 = \frac{1}{2} \log \left(\frac{\Gamma_0}{\Sigma_0} \kappa_1 \right). \tag{51}$$

7 Existence via Geometric theory of singular perturbations

This section is devoted to proving the existence of a heteroclinic orbit $\chi(\eta)$ with limiting behavior as determined in section 6.

Theorem 1. *Let (α, m, n) take values in the range (23). Given $\lambda > 0$ satisfying (43) with $n = 0$, there is $n_0(\lambda, \alpha, m)$ such that for $n \in [0, n_0)$ and λ satisfying (43) the system (S) admits a heteroclinic orbit $\chi^{\lambda, \alpha, m, n}(\eta)$ joining the equilibrium $M_0^{\lambda, \alpha, m, n}$ to the equilibrium $M_1^{\lambda, \alpha, m, n}$ and satisfying the property*

$$e^{-2\eta} \left(\chi^{\lambda, \alpha, m, n}(\eta) - M_0^{\lambda, \alpha, m, n} \right) \to \kappa X_{01}^{\lambda, \alpha, m, n} \quad \text{as } \eta \to -\infty \text{ for some } \kappa \neq 0. \tag{52}$$

The heteroclinic orbit $\chi^{\lambda,\alpha,m,n}(\eta)$ is achieved by applying the *geometric singular perturbation theory*. The presence of the small parameter $n > 0$ in the left-hand-side of (S)$_3$ provides a *fast-slow* structure to the system, having r as a fast variable and the rest as slow variables. In the interest of the reader, we present some preliminary information. Experts on geometric singular perturbation theory may wish to proceed directly to Sections 7.2, 7.3.

Recall that (S) accounts for a family of dynamical systems parametrized by (λ, α, m, n); the heteroclinic orbit will be achieved respectively for each admissible (λ, α, m, n). To simplify notations we suppress the dependence on λ, α, and m but retain the dependence on n.

7.1 Invariant manifold theory and geometric singular perturbation theory

We state here some rudiments of the geometric singular perturbation theory from [11, 12]. Fenichel's persistence theorem is developed in [12, Theorem 9.1]. In the present application the versions [25, Theorem 2.2] and [25, Theorem 3.1] are applied.

Let X be a C^r vector field in $\mathbb{R}^d$ with $r \geq 2$ and let $\bar{\Lambda} = \Lambda \cup \partial\Lambda$ be a compact, connected C^{r+1} manifold in $\mathbb{R}^d$. $F^t : \mathbb{R}^d \mapsto \mathbb{R}^d$ denotes the time t-map associated with the vector field X and DF^t denotes its differential. $\bar{\Lambda}$ is said to be *overflowing invariant* under X if for every $m \in \bar{\Lambda}$ and $t \leq 0$, $F^t(m) \in \bar{\Lambda}$ and X is pointing strictly outward on $\partial\Lambda$. $T\mathbb{R}^d|\bar{\Lambda}$ denotes the tangent bundle of $\mathbb{R}^d$ along $\bar{\Lambda}$ and $T\bar{\Lambda}$ denotes the tangent bundle of $\bar{\Lambda}$. A subbundle $E \subset T\mathbb{R}^d|\bar{\Lambda}$ is said to be negatively invariant if $E \supset DF^t(E)$ for all $t \leq 0$.

Let $E \subset T\mathbb{R}^d|\bar{\Lambda}$ be a subbundle that is negatively invariant and contains $T\bar{\Lambda}$. Given such E, $T\mathbb{R}^d|\bar{\Lambda}$ then splits into $T\mathbb{R}^d|\bar{\Lambda} = E \oplus E' = T\bar{\Lambda} \oplus N \oplus E'$, where $N \subset E$ is any complement of $T\bar{\Lambda}$ in E and $E' \subset T\mathbb{R}^d|\bar{\Lambda}$ is any complement of E in $T\mathbb{R}^d|\bar{\Lambda}$. Next, the subbundles are distinguished according to the growth or decay rates of the linearized flow as $t \to -\infty$, following [12]: Let $m \in \bar{\Lambda}$ and $v^0 \in T_m\Lambda$; $w^0 \in N_m$; $x^0 \in E'_m$; $v^t = DF^t(m)v^0$; $w^t = \pi^N DF^t(m)w^0$; $x^t = \pi^{E'} DF^t(m)x^0$, where π^N and $\pi^{E'}$ are bundle projections onto N and E' respectively. Define

$$\nu^s(m) \triangleq \inf \left\{ \nu > 0 \ : \ \frac{1}{|x^{-t}|} = o(\nu^t) \quad \text{as } t \to \infty \quad \forall x^0 \in E'_m \right\}.$$

If $\nu^s(m) < 1$, define

$$\sigma^s(m) \triangleq \inf \left\{ \sigma > 0 \ : \ |v^{-t}| = o(|x^{-t}|^\sigma) \quad \text{as } t \to \infty \quad \forall x^0 \in E'_m, v^0 \in T_m\Lambda \right\}.$$

Next, define

$$\alpha^u(m) \triangleq \inf \left\{ \alpha > 0 \ : \ |w^{-t}| = o(\alpha^t) \quad \text{as } t \to \infty \quad \forall w^0 \in N_m \right\}.$$

If $\alpha^u(m) < 1$, define

$$\rho^u(m) \triangleq \inf \left\{ \rho > 0 \ : \ \frac{|w^{-t}|}{|v^{-t}|} = o(\rho^t) \quad \text{as } t \to \infty \quad \forall w^0 \in N_m, v^0 \in T_m\Lambda \right\}.$$

If $\rho^u(m) < 1$, define

$$\tau^u(m) \triangleq \inf \left\{ \tau > 0 \ : \ |\hat{v}^{-t}| = o\left(\left(\frac{|v^{-t}|}{|w^{-t}|} \right)^\tau \right) \quad \text{as } t \to \infty \quad \forall w^0 \in N_m, v^0 \in T_m\Lambda, \hat{v}^0 \in T_m\Lambda \right\}.$$

Definition 7.1. *Let $\bar{\Lambda} = \Lambda \cup \partial\Lambda$ be an overflowing invariant manifold such that $T\mathbb{R}^d|\bar{\Lambda}$ admits a splitting by E as described above. We say an overflowing invariant manifold $\bar{\Lambda}$ satisfies assumptions (A_r) and $(B_{r'})$, $r' \leq r - 1$ if for all $m \in \bar{\Lambda}$ the growth rates hold*

$$\nu^s(m) < 1, \quad \sigma^s(m) < \frac{1}{r}, \tag{A_r}$$

$$\alpha^u(m) < 1, \quad \rho^u(m) < 1, \quad \tau^u(m) < \frac{1}{r'}. \tag{$B_{r'}$}$$

18

Remark 7.1. Given the bundle splitting, the conditions (A_r) and $(B_{r'})$ suffice to construct the unstable manifold of $\bar{\Lambda}$ as well as the finer foliation structure within it; see [10, Theorem 4] and [11, Theorem 3]. Moreover, for the special case $E = T\bar{\Lambda}$, Fenichel in [9] proved the persistence of the overflowing manifold $\bar{\Lambda}$ of X_0 when only (A_r) is assumed.

Next, suppose that a C^r family of vector fields X_ϵ is given depending on a small parameter for $\epsilon \in [-\epsilon_0, \epsilon_0]$ is given. If $\bar{\Lambda}_\epsilon$ exists as a C^r family of overflowing invariant manifolds for each sufficiently small ϵ, then the unstable manifold and its foliation structure are persistent in an appropriate sense; see section 16 of [12], and the discussion in [12, p. 90].

Next, we introduce the notion of normal hyperbolicity for manifolds without boundary, [12, p.89] and [9, p.221].

Definition 7.2 (Normally Hyperbolic Invariant Manifold [12]). *Let Λ be a compact, invariant under X manifold without boundary. Let E^s and E^u be subbundles of $T\mathbb{R}^d|\Lambda$ such that $E^s + E^u = T\mathbb{R}^d|\Lambda$, $E^s \cap E^u = T\Lambda$, E^u is negatively invariant under X and E^s is negatively invariant under $-X$. We say Λ is r-normally hyperbolic if Λ is an overflowing invariant manifold with a subbundle E^u satisfying the rate assumptions (A_r) and Λ is so with E^s under $-X$.*

The geometric singular perturbation theory [12, Theorem 9.1] applies the invariant manifold theory to the *fast-slow* structure induced by the dynamical system

$$\begin{cases} \dot{x} = f(x, y, \epsilon), \\ \epsilon\dot{y} = g(x, y, \epsilon), \end{cases} \quad \text{where } \epsilon \in (-\epsilon_0, \epsilon_0), \epsilon_0 > 0 \text{ small}, \ x \in \mathbb{R}^\ell, \ y \in \mathbb{R}^k, \ \ell + k = d. \tag{53}$$

We say x is a slow variable and y is a fast variable. We assume that f and g are sufficiently smooth, and the terms slow and fast variable originate from the two limiting asymptotic problems :

$$\text{(Reduced Problem)} \quad \begin{cases} \dot{x} = f(x, y, 0), \\ 0 = g(x, y, 0), \end{cases} \qquad \text{(Layer Problem)} \quad \begin{cases} x' = 0, \\ y' = g(x, y, 0), \quad (\cdot)' = \dfrac{d}{d(t/\epsilon)}. \end{cases}$$

The zeroset $\mathscr{S}$ of $g(x, y, 0)$ defines a manifold the orbits of the Reduced problem take values. In general, $\mathscr{S}$ is not realized as a graph as it can have many branches. This manifold consists of equilibria of the Layer problem. We consider

$$\mathscr{S} = \Big\{ (x, y) \ \Big| \ g(x, y, 0) = 0 \Big\},$$

$$\mathscr{S}_R \subset \Big\{ (x, y) \in \mathscr{S} \ \Big| \ D_y g(x, y, 0) \text{ has the full rank } k \Big\} \quad \text{open},$$

$$\mathscr{S}_H \subset \Big\{ (x, y) \in \mathscr{S}_R \ \Big| \ \text{all eigenvalues of } D_y g(x, y, 0) \text{ have nontrivial real parts} \Big\} \quad \text{open}.$$

On $\mathscr{S}_R$, the equation $0 = g(x, y, 0)$ is locally solvable for y in terms of x and we speak of the reduced vector field X_R on slow variables. (See equation (7.8) in [12].) On a compact subset $K \subset \mathscr{S}_H$ Fenichel's persistence Theorem [12, Theorem 9.1] applies.

In the sequel, we need the notion of transversal intersections:

Definition 7.3 (Transversal Intersection). *([25, Definition 3.1]) Let $\mathscr{M}_1$ and $\mathscr{M}_2$ be submanifolds of a manifold $\mathscr{M}$. The manifolds $\mathscr{M}_1$ and $\mathscr{M}_2$ intersect transversally at a point $m \in \mathscr{M}_1 \cap \mathscr{M}_2$ iff*

$$T_m\mathscr{M} = T_m\mathscr{M}_1 + T_m\mathscr{M}_2$$

holds, where $T_m\mathscr{M}$ denotes the tangent space of the manifold $\mathscr{M}$ and similarly for $\mathscr{M}_1$ and $\mathscr{M}_2$.

It is shown in [25] that when heteroclinic orbits are realized as transversal interesections of a stable and an unstable manifold they are persistent under perturbations.

19

7.2 Singular orbits for the inviscid system with $n = 0$

Let us describe how we apply the perturbation theory to the case of (S). We take two normally hyperbolic manifolds $\mathcal{N}_0$ and $\mathcal{N}_1$, which are simply the equilibrium points M_0 and M_1. The goal of this section is to establish the transversal intersection of the $\mathcal{N}_0^u$, the unstable manifold of $\mathcal{N}_0$ in $pqrs$-space, and $\mathcal{N}_1^s$, the stable manifold of $\mathcal{N}_1$.

A bunch of symbols and series of notations, following [25], are introduced and used for the remaining section. $K \subset \mathscr{S}_H$ denotes a compact critical manifold to be specified later. The reduced vector field problem is defined in K and X_R denotes the reduced vector field. As the reduced vector field is defined in K, K may contain a finer invariant manifold $\mathcal{N}' \hookrightarrow K$ that is normally hyperbolic to the reduced vector field. As usual $\mathcal{N}'$, $W^u(\mathcal{N}')$, and $W^s(\mathcal{N}')$ will be respectively the manifold, its unstable, and its stable manifolds embedded in K. In particular, W_0^u denotes the reduced unstable manifold of $\mathcal{N}_0$ and W_1^s denotes the reduced stable manifold of $\mathcal{N}_1$ embedded in K. Inside of $W^u(\mathcal{N}')$ are foliations $\mathscr{F}_x^u$ (see [12, Theorem 12.2]), meaning a foliation that passes through $x \in W^u(\mathcal{N}')$. $\mathscr{F}_x^s$ stands for the analogous foliation of $W^s(\mathcal{N}')$. Finally, when geometric objects are extended via the invariant manifold theory, those objects for $n > 0$ are denoted by a superscript n, for example K^n, $\mathcal{N}_0^n$, $\mathcal{N}_0^{u,n}$, $W_0^{u,n}$, M_0^n, $\cdots$.

Next, we identify the Reduced problem,

$$
\begin{aligned}
\dot{p} &= p\Big(\frac{1}{\lambda}(r - a) + 2 - \lambda pr - q\Big), \\
\dot{q} &= q\Big(1 - \lambda pr - q\Big) + bpr, \\
0 &= r\Big(\frac{\alpha - m}{\lambda(1 + \alpha)}(r - a) + \lambda pr + q + \frac{\alpha}{\lambda}r\big(s - \frac{1 + m}{1 + \alpha}\big)\Big), \\
\dot{s} &= s\Big(\frac{\alpha - m}{\lambda(1 + \alpha)}(r - a) + \lambda pr + q - \frac{1}{\lambda}r\big(s - \frac{1 + m}{1 + \alpha}\big)\Big),
\end{aligned} \tag{R}
$$

and the Layer problem for the system (S),

$$
p' = 0, \quad q' = 0, \quad r' = r\Big(\frac{\alpha - m}{\lambda(1 + \alpha)}(r - a) + \lambda pr + q + \frac{\alpha}{\lambda}r\big(s - \frac{1 + m}{1 + \alpha}\big)\Big), \quad s' = 0. \tag{54}
$$

Here, $(\cdot)' = \frac{d}{d\tilde{\eta}} := \frac{d}{d(\eta/n)}$ denotes differentiation with respect to the fast independent variable $\tilde{\eta}$. The zero-set of the function

$$
g(p, q, r, s) \triangleq r\Big(\frac{\alpha - m}{\lambda(1 + \alpha)}(r - a) + \lambda pr + q + \frac{\alpha}{\lambda}r\big(s - \frac{1 + m}{1 + \alpha}\big)\Big) \tag{55}
$$

consists of the equilibria of (54).

7.2.1 Choice of the critical manifold K

The algebraic equation $g(p, q, r, s) = 0$ specifies three dimensional hypersurfaces. Away from the $r \equiv 0$ plane, one may obtain the hypersurface as a graph of the function

$$
r = \hat{r}(p, q, s) = \frac{\frac{\alpha - m}{\lambda(1 + \alpha)}a - q}{\frac{\alpha - m}{\lambda(1 + \alpha)} + \lambda p + \frac{\alpha}{\lambda}\big(s - \frac{1 + m}{1 + \alpha}\big)},
$$

or implicitly in the form

$$
\frac{\alpha - m}{\lambda(1 + \alpha)}(\hat{r} - a) + \lambda p\hat{r} + q + \frac{\alpha}{\lambda}\hat{r}\big(s - \frac{1 + m}{1 + \alpha}\big) = 0. \tag{56}
$$

The level sets of $\hat{r}$ can be used in the pqs-space in order to visualize the hypersurface; they are affine due to (56). Fig. 3 illustrates a few marked affine surfaces of $\hat{r}(p, q, s) = R$, in the range $0 \leq R \leq a$.
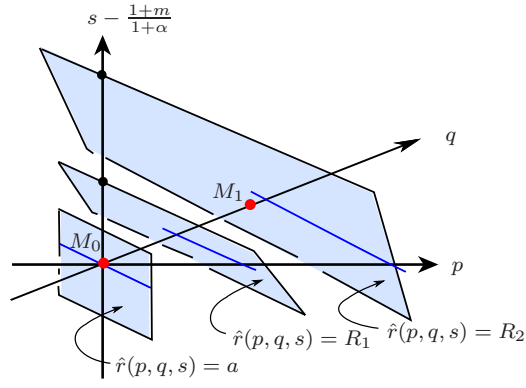
20

Figure 3: Affine level sets $\hat{r}(p, q, s) = R$, $0 \leq R \leq a$ in pqs-space

When $R = a(= r_0)$, it passes through $\left(0, 0, \frac{1+m}{1+\alpha}\right)$, which is the equilibrium M_0. As R decreases the affine level sets sweep the positive p, q sector. The surface crosses the other equilibrium M_1 when $R = r_1$. Then R continues to decrease until it touches the $r \equiv 0$ plane.

The critical manifold K is selected taking account of the properties of $\hat{r}(p, q, r)$. The domain of $\hat{r}$ is a trapezoid in pqs-space

$$D \triangleq \left\{ (p, q, s) \,\Big|\, p \geq -\epsilon, \;\; |q| \leq 2, \;\; \left|s - \frac{1+m}{1+\alpha}\right| \leq \frac{1}{2} \min\left\{\frac{\alpha-m}{\alpha(1+\alpha)}, \frac{1+m}{(1+\alpha)}\right\}, \right.$$
$$\left. \hat{r}(p, q, s) \geq \frac{1}{2} \min\{1, r_1\} \right\}.$$

where ϵ is a positive parameter selected sufficiently small. K is then defined by setting $K \triangleq \left(D, \hat{r}(D)\right)$. Note that K is chosen so that (i) M_0 and M_1 are on K; (ii) s and $r = \hat{r}(p, q, s)$ have positive lower bound
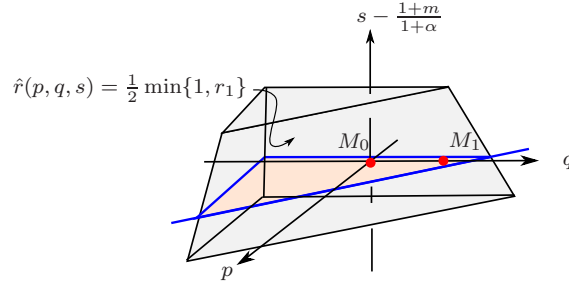

Figure 4: The trapezoid D, the domain of the graph.

on K. See the trapezoid D in Fig. 4.

Next, we verify that $K \subset \mathscr{S}_H$.

Proposition 7.1. *We have that* $K \subset \mathscr{S}_H$, *i.e., the partial jacobian* $\frac{\partial g}{\partial r}(p, q, r, s)|_{r=\hat{r}(p,q,s)} > 0$ *for all* $(p, q, r, s) \in K$.

Proof.

$$\frac{\partial g}{\partial r}\bigg|_K = \left(\frac{\alpha-m}{\lambda(1+\alpha)}(\hat{r} - a) + \lambda p \hat{r} + q + \frac{\alpha}{\lambda}\hat{r}\left(s - \frac{1+m}{1+\alpha}\right)\right) + \hat{r}\left(\frac{\alpha-m}{\lambda(1+\alpha)} + \lambda p + \frac{\alpha}{\lambda}\left(s - \frac{1+m}{1+\alpha}\right)\right)$$
$$= \hat{r}\left(\frac{\alpha-m}{\lambda(1+\alpha)} + \lambda p + \frac{\alpha}{\lambda}\left(s - \frac{1+m}{1+\alpha}\right)\right) \geq \frac{1}{2}\min\{1, r_1\}\left(\frac{\alpha-m}{2\lambda(1+\alpha)} - \lambda\epsilon\right).$$

It suffices to take $\epsilon < \frac{\alpha-m}{4\lambda^2(1+\alpha)}$, independently of n. $\qquad\qquad\square$

21

7.2.2 Nested invariant manifold structures in K

The flow (R), strictly restricted on K, is further analyzed. The three dimensional flow

$$
\begin{aligned}
\dot{p} &= p\Big(\frac{D}{\lambda(1+\alpha)}(\hat{r}-a_0) + \frac{\alpha}{\lambda}\hat{r}\big(s - \frac{1+m}{1+\alpha}\big)\Big), \\
\dot{q} &= q\Big(1 - \lambda p\hat{r} - q\Big) + bp\hat{r}, \\
\dot{s} &= -\frac{1+\alpha}{\lambda}\hat{r}s\Big(s - \frac{1+m}{1+\alpha}\Big).
\end{aligned}
\tag{R'}
$$

augmented in the r-direction by $r = \hat{r}(p,q,s)$ is the flow of the Reduced system (R).

It is necessary to pinpoint a few finer invariant structures of the reduced flow (R'), on which the invariant manifold theory can equally well be applied. This will be crucial ingredient of our arguments. To summarize, in the three dimensional reduced space K, we consider the embeddings

$$
M_0, M_1 \quad \hookrightarrow \quad p \equiv 0 \text{ line on } s \equiv \tfrac{1+m}{1+\alpha} \text{ plane} \quad \hookrightarrow \quad s \equiv \tfrac{1+m}{1+\alpha} \text{ plane} \quad \hookrightarrow \quad K,
$$

which consist of manifolds all of which are invariant under the flow (R'). Indeed, on the plane $s \equiv \frac{1+m}{1+\alpha}$, (R') decouples,

$$
\begin{aligned}
\dot{p} &= p\Big(\frac{D}{\lambda(1+\alpha)}(\hat{r}-a_0)\Big), \\
\dot{q} &= q\Big(1 - \lambda p\hat{r} - q\Big) + bp\hat{r},
\end{aligned}
\tag{57}
$$

where $\hat{r} = \hat{r}\big(p,q,\frac{1+m}{1+\alpha}\big)$. Restricting to $p \equiv 0$ we obtain yet another invariant line and importantly this line contains the equilibrium points M_0 and M_1.
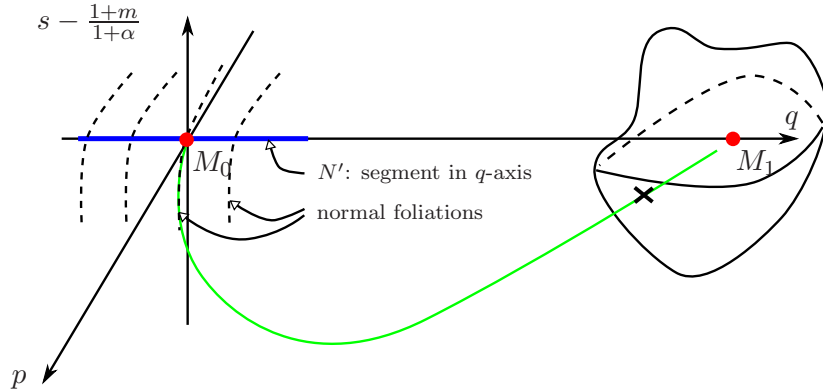

Figure 5: Nested invariant manifold structures

Fig. 5 illustrates the rest of the program. The justification of the following descriptions will be the subject of the next section. M_1 is a stable node; the three dimensional volume surrounding M_1 in Fig. 5 depicts its stable manifold. M_0 is a saddle; M_0 has two unstable dimensions in $s \equiv \frac{1+m}{1+\alpha}$, and has one stable dimension in its oblique direction. The vector aligned to q-axis and the one to the green orbit are two eigenvectors for the unstable dimensions. This explains how our heteroclinic orbit (the green one) appears in K.

Not all of the manifolds appearing are *normally hyperbolic* to the reduced vector field (R'): M_0 and M_1 are hyperbolic equilibrium points; $\hat{\mathcal{N}}^0$, a segment of $p \equiv 0$ line (the blue portion in Fig. 5) will be identified as an overflowing manifold satisfying the rate assumptions (A_r) and $(B_{r'})$. However, the plane $s \equiv \frac{1+m}{1+\alpha}$, in general, does not satisfy the necessary rate assumptions. See Remark 7.2

7.2.3 Analysis of the flow of (R′).

In the phase space K, the flow of (R′) can be completely analyzed. We visualize the overall flow by first analyzing the flow when restricted to the invariant plane $s \equiv \frac{1+m}{1+\alpha}$, and then noting that off the invariant plane the flow amounts to a stable relaxation process towards the invariant plane at $s \equiv \frac{1+m}{1+\alpha}$, see Fig. 6. The flow in the plane $s \equiv \frac{1+m}{1+\alpha}$ is characterized by using planar dynamical systems theory.
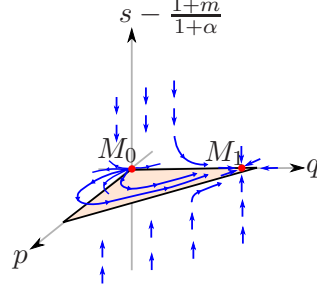

Figure 6: Flow on and around $s \equiv \frac{1+m}{1+\alpha}$

Remark 7.2. The property that the invariant plane $s \equiv \frac{1+m}{1+\alpha}$ has one stable direction in K may lead one to believe that the plane is normally hyperbolic. Indeed, the plane $s \equiv \frac{1+m}{1+\alpha}$ admits a splitting $T\mathbb{R}^3 = T\bar{\Lambda} \oplus E^s$ with the normal direction decaying. However, the notion of normal hyperbolicity requires stronger properties than merely admitting a splitting: Note that in (A_r) and $(B_{r'})$ upon a given splitting we demand $\sigma^s < 1/r$ and $\rho^u < 1/r'$. The latter for example leads to demanding that the negative eigenvalue μ_{14} of M_1 is strictly less than all other negative eigenvalues, which is not always the case. As a consequence, the persistence Theorem does not apply and we do not assert its persistence under perturbations.

We turn to the reduced linear stability of M_0 and M_1 in *pqs*-space. To summarize, the expressions in Section 5 also hold for $n = 0$, with the exception that the third eigenvalue μ_{03} and the third eigenvector X_{03} of M_0 (μ_{13} and X_{13} respectively of M_1) are no longer used. Indeed when $n = 0$, the flow is restricted on the three dimensional set K.

The following Lemma utilizes planar dynamical systems theory to characterizes the flow on a triangle T in the *pq*-plane.

Lemma 7.1. *Let T be the closed triangle on $s \equiv \frac{1+m}{1+\alpha}$ enclosed by $p = 0$, $q = 0$, and the level set $\hat{r}(p, q, \frac{1+m}{1+\alpha}) = \frac{1}{2}\min\{1, r_1\}$ that is intersected by $s \equiv \frac{1+m}{1+\alpha}$. Then $T \setminus M_0 \subset W^s(M_1)$.*

Proof. T is a two dimensional compact positively invariant set: (1) on $p = 0$, $\nu = (1, 0)$ and $X_R \cdot \nu = \dot{p} = 0$, where X_R stands for the reduced vector field of (R′); (2) on $q = 0$, $\nu = (0, 1)$ and $X_R \cdot \nu = \dot{q} = bp\hat{r} \geq 0$ (b in (21) is always positive); lastly on the hypotenuse, let $\underline{r} = \frac{1}{2}\min\{1, r_1\}$. The inward normal vector is $\nu = (-\lambda\underline{r}, -1)$. We compute

$$X_R \cdot \nu = -\lambda\underline{r}\dot{p} - \dot{q} = -\lambda\underline{r}p\left(1 - \lambda\underline{r}p - q + \frac{1}{\lambda}(\underline{r} - a) + 1\right) - q(1 - \lambda\underline{r}p - q) - b\underline{r}p$$

$$= (1 - \lambda\underline{r}p - q)(-\lambda\underline{r}p - q) - \underline{r}p\left((\underline{r} - a) + \lambda + b\right)$$

$$= \left(\frac{\alpha - m}{\lambda(1 + \alpha)}\right)^2 (\underline{r} - r_0)(\underline{r} - r_1) + \underline{r}p(1 - \underline{r}) \geq \delta > 0. \tag{58}$$

Let Ω be an ω-limit set of the orbit from $x_0 \in T \setminus M_0$. It is non-empty because T is compact. It cannot contain M_0, because for the flow restricted in T, M_0 does not have a stable manifold. It cannot contain a periodic orbit; if it did then there would be a fixed point in the interior of T and this is not the
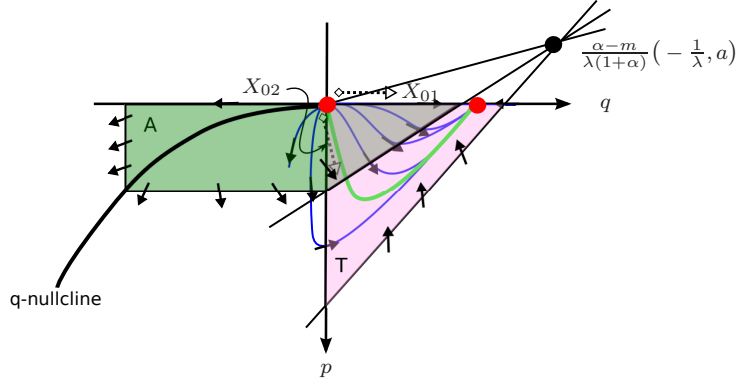
23

Figure 7: The schematic sketch of the flow on the invariant plane $s = \frac{1+m}{1+\alpha}$. Restricted on $s = \frac{1+m}{1+\alpha}$, M_0 is an unstable node and M_1 is a stable node. Two directions of unstable subspaces of M_0 are denoted by X_{01} and X_{02}; the straight lines emanating from the point $\frac{\alpha-m}{\lambda(1+\alpha)}\left(-\frac{1}{\lambda}, a\right)$ are the intersections of the level sets of $\hat{r}$ with the plane $s = \frac{1+m}{1+\alpha}$; the curve in the fourth quadrant is the nullcline of the equation $(\mathrm{R}')_2$; the triangle T is a 2-dimensional positively invariant set; the trapezoid A is a 2-dimensional negatively invariant set; the ω-limit set of any point in T is M_1; the α-limit set of any point in A is M_0; in particular there is a heteroclinic orbit (green one) that emanates from M_0 in the direction X_{01} lying in the strongly unstable manifold of M_0.

case. It cannot contain a separatrix cycle because T has only two fixed points M_0 and M_1 and again M_0 does not have a stable manifold. By Poincaré-Bendixson Theorem, the ω-limit set is M_1. □

Now we are able to state: We call $\mathscr{F}^u_{M_0} \subset W^u_0$ the strongly unstable manifold of M_0 satisfying (52) (the green line in Fig. 5) that is characterizable by the Unstable manifold theorem for the hyperbolic fixed point. That $\mathscr{F}^u_{M_0}$ ends up arriving at M_1 follows by Lemma 7.1, and this gives the proof for $n = 0$ of Theorem 1. The following proposition shows that the one dimensional manifold $\mathscr{F}^u_{M_0} \subset W^u_0$ intersects the three dimensional manifold $W^s_1 (= W^s(M_1))$ transversally (see Fig. 5).

Proposition 7.2. *Let $\mathscr{N}_0 = M_0$, $\mathscr{N}_1 = M_1$, $\mathscr{F}^u_{M_0} \subset W^u_0$ the strongly unstable manifold of M_0 satisfying (52), $W^s_1 = \Phi_{-t_0}(W^s_{loc}(M_1))$, the time $-t_0$ image of the local stable manifold of M_1 for large enough $t_0 < \infty$. Then $\mathscr{F}^u_{M_0}$ intersects W^s_1 transversally in pqs-space.*

Proof of Proposition 7.2. For large enough $t_0 < \infty$, by Lemma 7.1 the orbit point $x \in \mathscr{F}^u_{M_0}$ must be attained in W^s_1 as an interior point. Therefore the tangent space $T_x W^s_1$ is the whole of $T_x \mathbb{R}^3$. Then the intersection with $\mathscr{F}^u_{M_0}$ is trivially transversal. □

7.3 Persistence for $n > 0$

Having set forth the critical manifold K in $\mathscr{S}_H$ and the reduced vector field X_R on K, the theorem of Fenichel holds in K; the family K^n of *slow manifolds* persistently exist provided n is sufficiently small. Now we show the finer hyperbolic structure of $\mathscr{F}^u_{M_0} \hookrightarrow K$.

Lemma 7.2. *Let $\mathscr{N}_0 = M_0$, $\mathscr{F}^u_{M_0} \subset W^u_0$ the strongly unstable manifold of M_0 satisfying (52). Then, for sufficiently small n, $\mathscr{F}^u_{M_0}$ perturbs in a C^{r-1} manner to $\mathscr{F}^{u,n}_{M^n_0}$ the strongly unstable manifold of M^n_0 satisfying (52).*

Proof. In the *pqs*-space we select the line segment $\hat{\mathscr{N}}^0$ that is the transversal intersection of the invariant plane $\left\{ (p, q, s) \mid p = 0 \text{ and } q \in [-\frac{1}{2}, \frac{1}{2}] \right\}$ and the unstable manifold W^u_0. $\hat{\mathscr{N}}^n$ is defined as the intersection of the same plane with $W^{u,n}_0$. We see that $\hat{\mathscr{N}}^0 = \left\{ (p, q, s) \mid p = 0, \ q \in [-\frac{1}{2}, \frac{1}{2}] \text{ and } s = \frac{1+m}{1+\alpha} \right\}$.

24

$\hat{\mathcal{N}}^0$ is the one dimensional orbit in W_0^u that is not strongly unstable. We claim that $\hat{\mathcal{N}}^0$ is an overflowing invariant manifold as in Definition 7.1 of the reduced problem. More precisely, it satisfies (A_r) and $(B_{r'})$ with $r' = r - 1$ and E the tangent pq-plane.

From (57), $\dot{q} = q(1-q)$ on q-axis, it is clear that $\hat{\mathcal{N}}^0$ is overflowing invariant. Let E be pq-plane along $\hat{\mathcal{N}}^0$ and E' be the lines parallel to the s-axis. Then, $T\mathbb{R}^3|\hat{\mathcal{N}}^0$ splits into three one dimensional bundles $T\hat{\mathcal{N}}^0 \oplus N \oplus E'$ with N complementary to $T\hat{\mathcal{N}}^0$ in E such that N_{M_0} is parallel to X_{01}. The asymptotic rates are determined at M_0 by the eigenvalues of M_0. At M_0, E'_{M_0} is the stable subspace with eigenvalue $-\mu_{04}$ and N_{M_0} and $T_{M_0}\hat{\mathcal{N}}^0$ are the unstable ones with $\mu_{01} = 2$ and $\mu_{02} = 1$ respectively. From these, we compute

$$\nu^s = e^{-\mu_{04}}, \quad \sigma^s = 0, \quad \alpha^u = e^{-2}, \quad \rho^u = e^{-1}, \quad \tau^u = 0.$$

Therefore, for the given family of overflowing manifolds $\hat{\mathcal{N}}^n$, the strongly unstable manifold and its foliations $\mathscr{F}^u(x, n) := \mathscr{F}_x^{u,n}$ exist as a C^{r-1} family in both arguments x and n. In turn, the foliation $\mathscr{F}^u(M_0^n, n)$ that passes through M_0^n is a C^{r-1} map in n. $\square$

Persistence of the stable manifold $W_1^s (= W^s(M_1))$ is a consequence of the classical stable manifold theorem. Theorem 1 follows in the same way as in [25, Theorem 3.1] by the transversal intersection.

Proof of Theorem 1. By the theorem of Fenichel, for given $(\lambda, \alpha, m, 0)$ satisfying (23) and (48), n_0 can be taken sufficiently small so that if $n \in [0, n_0)$ then (λ, α, m, n) satisfies (23) and (48) and the system (S) admits a transversal heteroclinic orbit joining equilibrium M_0^n to equilibrium M_1^n: $\mathscr{F}_{M_0}^u$ perturbs to $\mathscr{F}_{M_0^n}^{u,n}$ by Lemma 7.2 and W_1^s perturbs to $W_1^{s,n}$ and the transversal intersection is stable under the perturbation. $\square$

8 Emergence of localization

By transforming back using (24), (37), (39), and (42), we recover the profile $\big(\Gamma(\xi), V(\xi), \Theta(\xi), \Sigma(\xi)\big)$ and $U(\xi)$ by (27) and the associated solution. We replace $t \to t + 1$ to obtain the final expression:

$$\gamma(t, x) = (t+1)^a \Gamma((t+1)^\lambda x), \quad v(t, x) = (t+1)^b V((t+1)^\lambda x), \qquad \theta(t, x) = (t+1)^c \Theta((t+1)^\lambda x),$$
$$\sigma(t, x) = (t+1)^d \Sigma((t+1)^\lambda x), \quad u(t, x) = (t+1)^{b+\lambda} U((t+1)^\lambda x).$$

We interpret $\big(\Gamma(\xi), V(\xi), \Theta(\xi), \Sigma(\xi)\big) = \big(\gamma(0, x), v(0, x), \theta(0, x), \sigma(0, x)\big)|_{x=\xi}$ as the initial state. For given material parameters (α, m, n), there are two available degrees of freedom giving rise to a two-parameters family of solutions. As noted in Section 6.3, the choices of U_0 and Γ_0 determine the self-similar profile while the remaining boundary values (Θ_0, Σ_0) and the rate λ are induced by them. The range of U_0 and Γ_0 is such that

$$\frac{2(1+\alpha) - n}{D} < \frac{U_0}{\Gamma_0} < \frac{2(1+\alpha) - n}{D} + \frac{4(1+\alpha)(\alpha - m - n)(1+m)}{D(1+m+n)^2}.$$

The localizing rate λ satisfies (48) and takes values $0 < \lambda < \frac{2(\alpha - m - n)}{1 + m + n}\left(\frac{1+m}{1+m+n}\right)$. In the sequel, we establish properties of the profiles and the emergence of localization, in the sense of definition (5), (6).

8.1 Properties of the self-similar profiles

We first list some information on the behavior of the profiles near $\xi = 0$ and as $\xi \to \infty$. The latter determines the behavior of the induced solutions off the localization zone.

Proposition 8.1. *Let* $\big(\Gamma(\xi), V(\xi), \Theta(\xi), \Sigma(\xi)\big)$ *be the self-similar profiles defined by transformations of* (37), (39), (42) *from the heteroclinic orbit* $\chi(\eta) = \big(p(\eta), q(\eta), r(\eta), s(\eta)\big)$ *constructed in Theorem 1 in the range of parameters* $\Gamma(0) = \Gamma_0$ *and* $U(0) = U_0$ *depicted by* (49). $U(\xi)$ *is defined by* (27). *Then,*

(i) *The self-similar profile achieves the boundary condition at $\xi = 0$,*

$$V(0) = \Gamma_\xi(0) = \Theta_\xi(0) = \Sigma_\xi(0) = U_\xi(0) = 0, \quad \Gamma(0) = \Gamma_0, \quad U(0) = U_0.$$

(ii) *Its asymptotic behavior as $\xi \to 0$ is given by*

$$
\begin{aligned}
\Gamma(\xi) - \Gamma_0 &= \Gamma''(0)\frac{\xi^2}{2} + o(\xi^2), \quad \Gamma''(0) < 0, \\
\Theta(\xi) - c^{-\frac{1}{1+\alpha}}\Gamma_0^{\frac{m}{1+\alpha}}U_0^{\frac{1+n}{1+\alpha}} &= \Theta''(0)\frac{\xi^2}{2} + o(\xi^2), \quad \Theta''(0) < 0, \\
\Sigma(\xi) - c^{\frac{\alpha}{1+\alpha}}\Gamma_0^{\frac{m}{1+\alpha}}U_0^{-\frac{\alpha-n}{1+\alpha}} &= \Sigma''(0)\frac{\xi^2}{2} + o(\xi^2), \quad \Sigma''(0) > 0, \\
U(\xi) - U_0 &= U''(0)\frac{\xi^2}{2} + o(\xi^2), \quad U''(0) < 0, \\
V(\xi) - U_0\xi &= U''(0)\frac{\xi^3}{6} + o(\xi^3), \quad U''(0) < 0.
\end{aligned}
\tag{59}
$$

(iii) *Its asymptotic behavior as $\xi \to \infty$ is given by*
if $\mu_{11} \neq -1$, or $\mu_{11} = -1$ but $b = \lambda$,

$$
\begin{aligned}
\Gamma(\xi) = O\big(\xi^{-\frac{1+\alpha}{\alpha-m-n}}\big), \quad V(\xi) = O(1), \qquad \Theta(\xi) = O\big(\xi^{-\frac{1+m+n}{\alpha-m-n}}\big), \\
\Sigma(\xi) = O(\xi), \qquad U(\xi) = O\big(\xi^{-\frac{1+\alpha}{\alpha-m-n}}\big)
\end{aligned}
\tag{60}
$$

otherwise

$$
\begin{aligned}
\Gamma(\xi) &= O\big(\xi^{-\frac{1+\alpha}{\alpha-m-n}}\big(\log\xi\big)^{\frac{1+\alpha}{D}}\big), \qquad V(\xi) = O\big(\big(\log\xi\big)^{-\frac{\alpha-m-n}{D}}\big), \\
\Theta(\xi) &= O\big(\xi^{-\frac{1+m+n}{\alpha-m-n}}\big(\log\xi\big)^{\frac{1+m+n}{D}}\big), \\
\Sigma(\xi) &= O\big(\xi\big(\log\xi\big)^{-\frac{\alpha-m-n}{D}}\big), \qquad U(\xi) = O\big(\xi^{-\frac{1+\alpha}{\alpha-m-n}}\big(\log\xi\big)^{\frac{1+\alpha}{D}}\big)
\end{aligned}
\tag{61}
$$

Proof. The proof of the Proposition 6.1 and Remark 6.2 contains (i) and (ii) and thus we are left to prove (iii). In a similar fashion to (50), any orbit $\psi(\eta)$ in the local stable manifold of $W^s(M_1)$ is characterized by a triple $(\kappa_1', \kappa_2', \kappa_3')$ in association with the asymptotic expansion

$$
\begin{aligned}
&\psi(\eta) - M_1 \\
&= \begin{cases} \kappa_1' e^{\mu_{11}\eta}X_{11} + \kappa_2' e^{\mu_{12}\eta}X_{12} + \kappa_4' e^{\mu_{14}\eta}X_{14} + \text{high order terms} & \text{if } \mu_{11} \neq -1, \text{ or } \mu_{11} = -1 \text{ but } b = \lambda, \\ \kappa_1' \eta e^{\mu_{11}\eta}X_{11}' + \kappa_2' e^{\mu_{12}\eta}X_{12} + \kappa_4' e^{\mu_{14}\eta}X_{14} + \text{high order terms} & \text{if } \mu_{11} = \mu_{12} = -1 \text{ and } b \neq \lambda \end{cases}
\end{aligned}
\tag{62}
$$

as $\eta \to \infty$. The second formula reflects the presence of a generalized eigenvector.

Now, we have $q \to 1$, $r \to r_1$, $s \to s_1$ but $p \to 0$ and the leading order of p is to be found. We can determine the coefficient of X_{11}, above, because the p-component of the vectors X_{12} and X_{14} is 0. Since the plane $p \equiv 0$ is an invariant plane for a non-linear flow, triplets of the form $(0, \kappa_2', \kappa_3')$ spans this invariant plane. Because our heteroclinic orbit $\chi(\eta)$ ventures out from the plane $p \equiv 0$, κ_1' for the expansion of $\chi(\eta)$ cannot be 0. This implies that the leading order of $p(\log\xi)$ is

$$
p(\log\xi) = \begin{cases} O(\xi^{\mu_{11}}) & \text{if } \mu_{11} \neq -1 \text{ or } \mu_{11} = -1 \text{ but } b = \lambda, \\ O(\xi^{\mu_{11}}\log\xi) & \text{otherwise} \end{cases}
$$

as $\xi \to \infty$.

Asymptotics (60) and (61) are the straightforward calculations obtained from the reconstruction formulas

$$\tilde{\gamma} = p^{\frac{1+\alpha}{D}} r^{\frac{n}{D}} s^{\frac{\alpha}{D}}, \qquad \tilde{v} = \frac{1}{b} p^{-\frac{\alpha-m-n}{D}} q r^{\frac{n}{D}} s^{\frac{\alpha}{D}}, \qquad \tilde{\theta} = p^{\frac{1+m+n}{D}} r^{\frac{2n}{D}} s^{-\frac{1-m-n}{D}},$$

$$\tilde{\sigma} = p^{-\frac{\alpha-m-n}{D}} r^{\frac{n}{D}} s^{\frac{\alpha}{D}}, \qquad \tilde{u} = p^{\frac{1+\alpha}{D}} r^{\frac{n}{D}+1} s^{\frac{\alpha}{D}},$$

via (37) and (39). □

8.2 Emergence of localization

As time proceeds, the initial nonuniformity evolves into localization. This section is devoted to describing the behavior of the various fields as time advances. We only present the generic case $-\frac{1+m+n}{\alpha-m-n} \neq -1$; in the non-generic case we would have to add a logarithmic correction according to Proposition 8.1.

- Strain : The strain keeps increasing as time proceeds. The growth at the origin is faster than the growth rate at all other points:

$$\gamma(t,0) = (1+t)^{\frac{2+2\alpha-n}{D}+\frac{2+2\alpha}{D}\lambda} \Gamma(0),$$

$$\gamma(t,x) \sim t^{\frac{2+2\alpha-n}{D}-\frac{(1+\alpha)(1+m+n)}{D(\alpha-m-n)}\lambda} |x|^{-\frac{1+\alpha}{\alpha-m-n}}, \quad \text{as } t \to \infty, \ x \neq 0.$$

Recall that the condition $\frac{2+2\alpha-n}{D} - \frac{(1+\alpha)(1+m+n)}{D(\alpha-m-n)}\lambda > 0$ was the ground for imposing (43), placed to guarantee that the plastic strain is growing even outside the localization zone. On the other hand, the difference between the rate of growth of γ at $x = 0$ and the rate at $x \neq 0$ is easily computed as $\frac{1+\alpha}{\alpha-m-n}\lambda > 0$, which indicates localization of the profile of γ around $x = 0$.

- Temperature : For the temperature , the growth at the origin is again faster than other points,

$$\theta(t,0) = (1+t)^{\frac{2(1+m)}{D}+\frac{2(1+m+n)}{D}\lambda} \Theta(0),$$

$$\theta(t,x) \sim t^{\frac{2(1+m)}{D}-\frac{(1+m+n)^2}{D(\alpha-m-n)}\lambda} |x|^{-\frac{1+m+n}{\alpha-m-n}}, \quad \text{as } t \to \infty, \ x \neq 0.$$

Again, the positivity of the growth rate $\frac{2(1+m)}{D} - \frac{(1+m+n)^2}{D(\alpha-m-n)}\lambda$ is a consequence of (43).

- Strain rate : The growth rates of the strain-rate is by definition less by one to those of the strain, again illustrating localization.

$$u(t,0) = (1+t)^{\frac{1+m}{D}+\frac{2+2\alpha}{D}\lambda} U(0),$$

$$u(t,x) \sim t^{\frac{1+m}{D}-\frac{(1+\alpha)(1+m+n)}{D(\alpha-m-n)}\lambda} |x|^{-\frac{1+\alpha}{\alpha-m-n}}, \quad \text{as } t \to \infty, \ x \neq 0.$$

- Stress : The stress decays with time at all points, but the decay at $x = 0$ is much faster than the decay in other places, indicating stress-collapse in the interior of the band:

$$\sigma(t,0) = (1+t)^{\frac{-2\alpha+2m+n}{D}+\frac{-2\alpha+2m+2n}{D}\lambda} \Sigma(0),$$

$$\sigma(t,x) \sim t^{\frac{-2\alpha+2m+n}{D}+\frac{1+m+n}{D}\lambda} |x|, \quad \text{as } t \to \infty, \ x \neq 0,$$

The difference of the two rates is $\left(\frac{1+m+n}{D} - \frac{-2\alpha+2m+n}{D}\right)\lambda = \lambda$.

- Velocity : The velocity is an odd function of x. At fixed t, $v(t,x)$ is an increasing function of x ranging from $-v_\infty(t)$ to $v_\infty(t)$, where $v_\infty(t) \triangleq \lim_{x \to \infty} v(t,x)$. The velocity field is contrasted with the linear field of uniform shear motion. The self-similar scaling $\xi = (1+t)^\lambda x$ implies that most

27

of the transition takes place around the origin leading eventually to step-function behavior as time goes to infinity. The asymptotic velocity is

$$v_\infty(t) = (1+t)^b V_\infty = (1+t)^{\frac{1+m}{D}+\frac{1+m+n}{D}\lambda} V_\infty, \quad V_\infty \triangleq \lim_{\xi \to \infty} V(\xi) < \infty.$$

Note that the far field loading condition is different from the linear profile of uniform shearing. This deviation is a consequence of our simplifying assumption of self-similarity.

9 Numerical computation of the heteroclinic orbit

In this section we present in detail the process we followed to capture numerically the heteroclinic orbit connecting M_0 and M_1. This is a challenging computational task since both M_0 and M_1 are saddle points and the heteroclinic orbit connecting them is the intersection of two 3-dimensional manifolds $W^u(M_0)$ and $W^s(M_1)$ in $\mathbb{R}^4$. Here, we use the software package $AUTO$, [6], [7], [8] to compute the heteroclinic orbit connecting M_0 and M_1. One of the main capabilities of $AUTO$ is that it can perform limited bifurcation analysis for parametric systems of ordinary differential equations of the form : $u'(t) = f(u(t), \chi)$ where $f(\cdot, \cdot)$, $u(\cdot) \in \mathbb{R}^d$ and χ could be one or a set of free parameters.

A direct application of $AUTO$ for solving system (S) and computing the desired heteroclinic orbit will fail. A more careful approach has to be considered, starting from some well prepared data and continuing by exploiting the continuation capabilities of $AUTO$. Indeed, we start with an exact solution of system (S) available for a specific value of the parameter α and variable p, followed by a projection and two continuation steps escaping from these particular choices for α and p allowing us to compute the heteroclinic orbit. We proceed by describing these four steps in detail.

9.1 Continuation by AUTO

Step 1. (Exact solution) The system (S) admits an explicit solution for certain values of the parameters α, n and the variable p. First for $\alpha = 0$ the equations for p, q, r in (S) decouple from the equation of s. This reduced system carries only the three dimensional unstable manifold of M_0 characterizing the heteroclinic orbit as a node-saddle connection. Hence, in principle, by running time backwards and using a shooting argument in a small neighbourhood of M_1, any heteroclinic orbit can be computed as accurate as the numerical time integrator allows. However we can be more precise and prepare the data even better by noticing that for $p \equiv 0$ the equation for q in (S) decouples completely from the rest and can be solved explicitly. Further, using this analytic value of q an exact solution can be also derived for r in the case when $n = \dfrac{1}{k}$, $k \geq 1$, $k \in \mathbb{Z}$:

$$\alpha = 0, \quad p \equiv 0, \quad q(\eta) = \frac{1}{1 + e^{-\eta}},$$

$$r(\eta) = \frac{r_0 \left(1 + e^\eta\right)^k}{\displaystyle\sum_{j=0}^{k} \frac{kW_0}{kW_0 - j} \binom{k}{j} e^{j\eta}}, \quad \text{where } W_0 = -\frac{(m+n)r_0}{\lambda}. \tag{63}$$

Step 2. (Projection step, $\alpha = 0$, $p \equiv 0$) At this step we integrate numerically the equation for s using the exact values of $q(\eta), r(\eta)$ found in the previous step. The integration can be performed by either $AUTO$ or any other numerical integrator. The integration timespan is chosen to be $\eta \in [-\eta_{max}, \eta_{max}]$ so that the starting point $(p, q, r, s)|_{\eta=-\eta_{max}}$ and the ending point $(p, q, r, s)|_{\eta=\eta_{max}}$ both fall in small neighbourhoods of M_0 and M_1 respectively. In particular we choose the starting point so that $(p, q, r, s)|_{\eta=-\eta_{max}} =$

$M_0 + \epsilon_0\nu_0$, $\nu_0 = X_{02}$ and ϵ_0 as small parameter. Using this an initial value we integrate numerically the following non-autonomous equation for s

$$\dot{s} = s\left(\frac{-m-n}{\lambda}(r(\eta) - a) + q(\eta) - \frac{1}{\lambda}r(\eta)\big(s - (1 + m + n)\big) - \frac{n}{\lambda}\right).$$

At the end of the calculation we project the vector $(p, q, r, s)|_{\eta=\eta_{max}} - M_1$ to the stable *subspace* of M_1. Indeed, we can find explicitly $\epsilon_1 \ll 1$ and $\nu_1 \in \mathrm{Span}\{X_{11}, X_{12}, X_{14}\}$, $|\nu_1| = 1$ such that $\pi\big((p, q, r, s)|_{\eta=\eta_{max}} - M_1\big) = \epsilon_1\nu_1$, where π denotes the projection. At the completion of Step 2 we have the solution $(p, q, r, s)(\eta), \eta \in [-\eta_{max}, \eta_{max}]$ at discrete levels $\eta_i, i = 0, \ldots N$ for $\alpha = 0$ and lying in the plane $p \equiv 0$.

Step 3. (Continuation with $\alpha \neq 0$, $p = 0$) The goal in this step is to create a set of orbits in the plane $p \equiv 0$ but with α not any more trivial. To that effect, we use the well prepared data obtained in Step 2 and we run $AUTO$ with ν_0 fixed but allowing $\alpha, m, \lambda, \epsilon_0, \epsilon_1, \nu_1$ be continued. The continuation process performed by $AUTO$ creates a family of orbits with the following characteristics : a) emanate from a small neighbourhood of size ϵ_0 of M_0 in the direction of ν_0, b) terminate in a small neighbourhood of size ϵ_1 of M_1, c) lie in the plane $p \equiv 0$ but with $\alpha \neq 0$.

Step 4. (Continuation with $\alpha \neq 0$, $p \neq 0$) In this step we capture the desired heteroclinic orbit connecting M_0 and M_1. From the family of orbits obtained in Step 3 we select one according to the physical relevance of the parameters α, m, n and λ. We run $AUTO$ again allowing ν_0 in span$\{X_{01}, X_{02}, X_{03}\}$ to be continued, thus leaving the plane $p \equiv 0$. $AUTO$ generates a family of orbits emanating from M_1, terminating in a neighbourhood of size ϵ_0 of M_0 and is the 2-surface of heteroclinic orbits of $W^u(M_0) \cap W^s(M_1)$. One of these orbits is the desired heteroclinic orbit with $\nu_0 = X_{01}$.

Remark 9.1. We note that the exact solution of r in (63) is valid only for values of n of the form $n = \frac{1}{k}$, $k \geq 1, k \in \mathbb{Z}$. In the case that n is not of this form then one can rely on an numerical integrator for solving as accurately as possible the equation for r using the exact value of q.

9.2 Numerical Results

In this section we illustrate the computation of the heteroclinic orbit of (S), following the steps described in detail above. Further, using the heteroclinic orbit (p, q, r, s) of system (S) we compute the associated self-similar solution in terms of the original variables $v(x, t), u(x, t), \theta(x, t), \sigma(x, t)$.

We begin by giving the explicit relation of the variables $(p(\eta), q(\eta), r(\eta), s(\eta))$ to the original variables $v(x, t), u(x, t), \theta(x, t), \sigma(x, t)$. Indeed, collecting the transformations and change of variables described in (24), (37) and (39), we obtain

$$v(x,t) = \frac{1}{b}t^b\, \xi^{-b_1}\, p^{\frac{(-\alpha+m+n)}{D}} s^{\frac{\alpha}{D}} r^{\frac{n}{D}} \qquad u(x,t) = t^{b+\lambda}\, \xi^{-b_1-1}\, p^{\frac{(1+\alpha)}{D}} s^{\frac{\alpha}{D}} r^{1+\frac{n}{D}}$$
$$\theta(x,t) = t^c\, \xi^{-c_1}\, p^{\frac{(1+m+n)}{D}} s^{\frac{m+n-1}{D}} r^{\frac{2n}{D}}, \qquad \sigma(x,t) = t^d\, \xi^{-d_1}\, p^{\frac{(-\alpha+m+n)}{D}} s^{\frac{\alpha}{D}} r^{\frac{n}{D}}$$

(64)

where $\eta = \log\xi$, $\xi = t^\lambda x$ and a, b, c, d, D as in (21), (22). We present now the results of three numerical experiments. All the computations where performed with $\eta_{max} = 10$ and $\lambda = \frac{1}{2}\lambda_{max}$ where λ_{max} is the upper bound of λ in (43). The initial values of α, m are taken as $\alpha = 0$ and $m = -0.6, -0.5, -0.5$, respectively. The corresponding values of n remained fixed throughout the process and were $n = 0.025, 0.0125, 0.01$. Following the process described in Section 9.1, the software $AUTO$ was able to perform the continuation process and capture the desired heteroclinic orbit. The resulting values for α and m are shown in the figures, along with the value of the parameter $L_p = -\alpha + m + n$. The change of sign of L_p from positive to negative signals the onset of localization.

Figures 8, 9 and 10 illustrate the emergence of localization by depicting the profiles of the original variables v, u, θ, σ at a few time instances. The vertical axes, except for the velocity v, are in logarithmic scale, however the corresponding $y-$range of values for each variable, is the same in all figures. In part
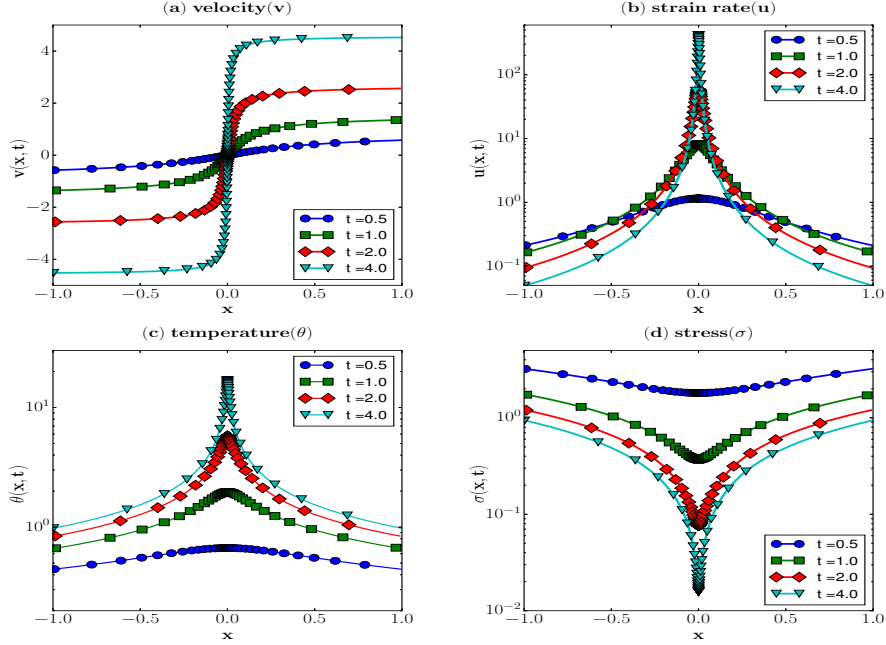
29

Figure 8: $\alpha = 1.572,\ m = 0.02246,\ n = 0.025,\ L_p = -1.52454$.

(a) of each figure the velocity profile is depicted, which eventually, attains the shape of a step function. Parts (b) and (c) of the figures present the localization in strain rate and temperature respectively. In both cases the initial profile is a small perturbation of a constant state which at later time localizes at the origin. On the other hand, part (d) of figures shows the collapse of the stress to zero. The rate of localization at the origin differs for each numerical experiment and depends on the values of the materials parameters α, m, n and L_p. In particular, the onset of localization is characterized by the parameter L_p taking a negative value. Further, the rate of localization is determined by the magnitude of this negative value, with larger negative values indicating faster localization, as it is observed in Figures 8-10.

There is the possibility of constructing the heteroclinic orbits via a shooting method, but this works only in the special cases $\alpha = 0$, $m < 0$ and $m = 0$, see [18] and [19] respectively. The shooting method does not work in the general case where all parameters are nonzero.

A   The loss of hyperbolicity for $n = 0$

Consider the system (1) when $n = 0$, that is the viscoplastic effects are neglected. Then (2) reads

$$\sigma = \tau(\theta, \gamma) = \theta^{-\alpha}\gamma^m \tag{65}$$

and (1) is written as a first order system

$$\begin{pmatrix} v_t \\ \theta_t \\ \gamma_t \end{pmatrix} = \underbrace{\begin{pmatrix} 0 & \tau_\theta(\theta, \gamma) & \tau_\gamma(\theta, \gamma) \\ \tau(\theta, \gamma) & 0 & 0 \\ 1 & 0 & 0 \end{pmatrix}}_{\triangleq\, B(\theta, \gamma)} \begin{pmatrix} v_x \\ \theta_x \\ \gamma_x \end{pmatrix}. \tag{66}$$
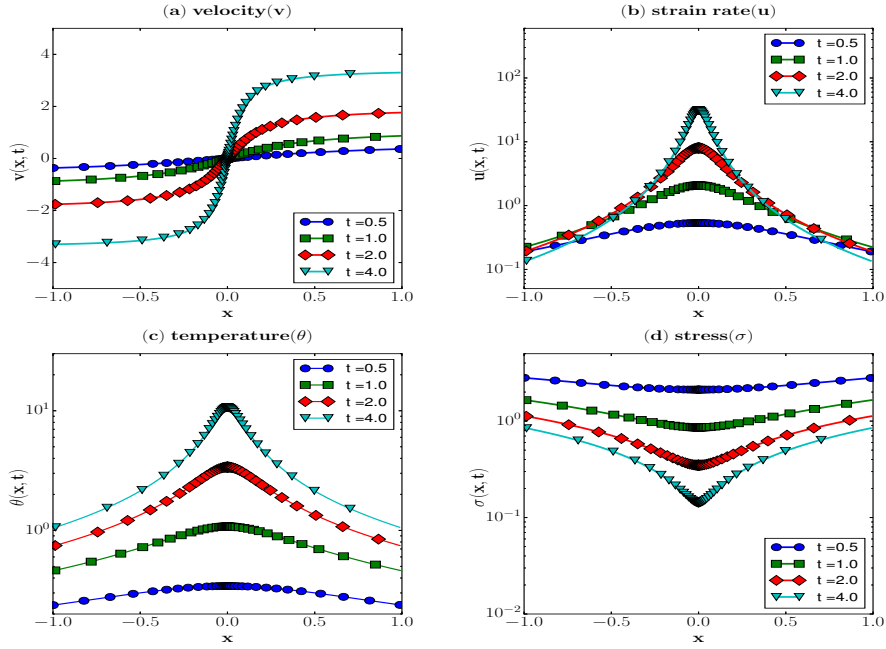
Figure 9: $\alpha = 1.1698,\ m = 0.2057,\ n = 0.0125,\ L_p = -0.9516.$

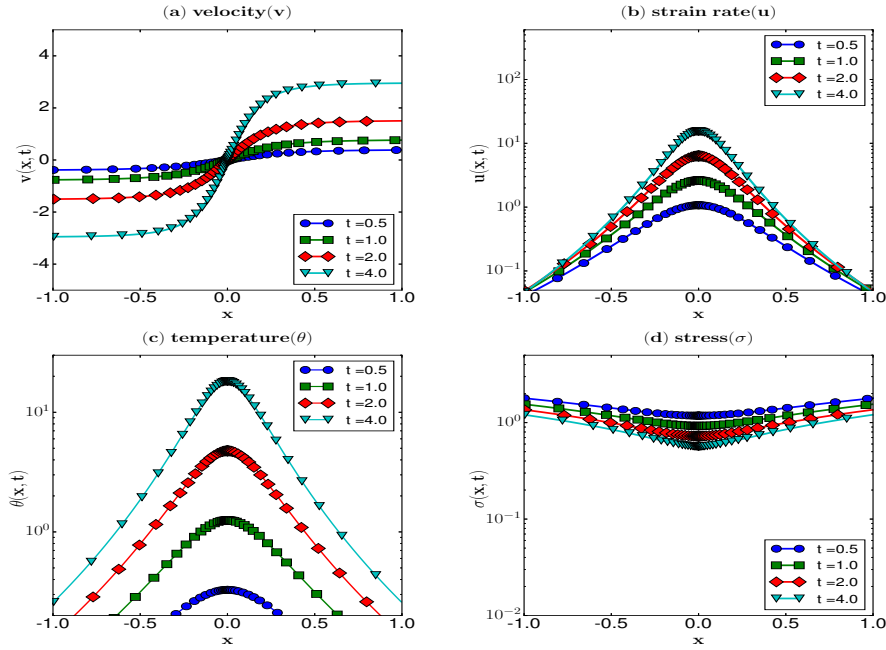Figure 10: $\alpha = 0.5957,\ m = 0.3437,\ n = 0.01,\ L_p = -0.242.$

We check hyperbolicity for (66). The characteristic speeds are the roots of

$$\det\left(B - \lambda \mathrm{I}\right) = -\lambda\left(\lambda^2 - (\tau_\theta \tau + \tau_\gamma)\right) = 0$$

The system is thus hyperbolic when $\tau_\theta \tau + \tau_\gamma > 0$ and elliptic in the t-direction when $\tau_\theta \tau + \tau_\gamma < 0$. Observe that along the evolution of (66) and under the conditions for loading of interest in our problem, we have that γ is increasing; the equation

$$\theta_t = \tau(\theta, \gamma)\gamma_t$$

implies that

$$\tau_\theta \tau + \tau_\gamma = \frac{d}{d\gamma}\tau(\theta, \gamma)\,.$$

We conclude that the system is hyperbolic before the maximum of the stress-strain curve, and elliptic beyond the maximum point. For the constitutive law (65) a computation shows

$$\tau_\theta \tau + \tau_\gamma = \theta^{-\alpha}\gamma^{m-1}\left(-\alpha\frac{\gamma^{m+1}}{\theta^{1+\alpha}} + m\right)$$

$$= \frac{-\alpha + m}{1 + \alpha} + \frac{\alpha(1 + m)}{\theta^{1+\alpha}}\left(\frac{\theta_0(x)^{1+\alpha}}{1 + \alpha} - \frac{\gamma_0(x)^{1+m}}{1 + m}\right)$$

In the region $\alpha > m$ the stress-strain curve may be initially increasing (depending on the data) but eventually decreases.

The system (66) admits the class of uniform shearing solutions

$$v_s(x) = x\,, \quad \gamma_s(t) = t + \gamma_0\,, \quad \theta_s(t) \text{ is determined by solving } \begin{cases} \frac{d\theta_s}{dt} = \tau(\theta_s, \gamma_s) \\ \theta_s(0) = \theta_0 \end{cases} \tag{67}$$

where γ_0, $\theta_0 >$ are the initial strain and temperature, respectively. We linearize around the uniform shearing solution by setting

$$v = x + \hat{V}(t, x)\,, \quad \theta = \theta_s(t) + \hat{\Theta}(t, x)\,, \quad \gamma = \gamma_s(t) + \hat{\Gamma}(t, x)$$

and obtain the linearized system satisfied by the perturbation $(\hat{V}, \hat{\Theta}, \hat{\Gamma})$,

$$\begin{pmatrix} \hat{V}_t \\ \hat{\Theta}_t \\ \hat{\Gamma}_t \end{pmatrix} = B(\theta_s(t), \gamma_s(t)) \begin{pmatrix} \hat{V}_x \\ \hat{\Theta}_x \\ \hat{\Gamma}_x \end{pmatrix} + \begin{pmatrix} 0 & 0 & 0 \\ 0 & \tau_\theta(\theta_s, \gamma_s) & \tau_\gamma(\theta_s, \gamma_s) \\ 0 & 0 & 0 \end{pmatrix} \begin{pmatrix} \hat{V} \\ \hat{\Theta} \\ \hat{\Gamma} \end{pmatrix}\,. \tag{68}$$

The above calculation shows that, when $\alpha > m$, the linearized system loses hyperbolicity in finite time, past the maximum of the curve $\sigma_s(t) - t$.

B The equilibria of the system (S)

We discussed in section 5 the equilibria M_0 and M_1 of (S). The remaining equilibria of (S) are listed below, and they are all functions of (α, m, n, λ) that lie outside the the sector

$$\mathscr{P} = \{(p, q, r, s) \mid p \geq 0,\ q \geq 0,\ r > 0,\ s > 0\}$$

in the parameter range (23). The reader will find underlined the components indicating that the equilibrium lies outside the sector of interest: We recall the notations

$$a = \frac{2 + 2\alpha - n}{D} + \frac{2(1 + \alpha)}{D}\lambda\,, \quad b = \frac{1 + m}{D} + \frac{1 + m + n}{D}\lambda\,, \quad D = 1 + 2\alpha - m - n$$

while t, t_1 and t_2 denote arbitrary real numbers.

$$
\begin{array}{ll}
(1) & \left(0,\ 0,\ \underline{0},\ \hspace{5em} \underline{0}\ \right), \\[4pt]
(2) & \left(0,\ 0,\ \underline{0},\ \hspace{5em} t\ \right) \quad \text{provided } \lambda = \frac{-2\alpha+2m+n}{2(\alpha-m-n)}, \\[4pt]
(3) & \left(0,\ 0,\ \frac{n\alpha-a(\alpha-m-n)}{(1+\alpha)(m+n)},\ \hspace{1.5em} \underline{0}\ \right), \\[4pt]
(4) & \left(0,\ 1,\ \underline{0},\ \hspace{5em} \underline{0}\ \right), \\[4pt]
(5) & \left(0,\ 1,\ \underline{0},\ \hspace{5em} t\ \right) \quad \text{provided } \lambda = \frac{2\alpha-2m-n}{1+m+n}, \\[4pt]
(6) & \left(0,\ 1,\ \frac{n\alpha-a(\alpha-m-n)}{(1+\alpha)(m+n)} + \frac{\lambda}{m+n},\ \underline{0}\ \right), \\[4pt]
(7) & \left(t,\ 0,\ \underline{0},\ \hspace{5em} \underline{0}\ \right) \quad \text{provided } \lambda = \frac{2+2\alpha-n}{2(\alpha-m-n)}, \\[4pt]
(8) & \left(t,\ 1,\ \underline{0},\ \hspace{5em} \underline{0}\ \right) \quad \text{provided } \lambda = \frac{-2-2\alpha+n}{1+m+n}, \\[4pt]
(9) & \left(t_1,\ 0,\ \underline{0},\ \hspace{5em} t_2\ \right) \quad \text{provided } 1+2\alpha-m-n=0 \text{ and } \lambda = \frac{-1-m}{1+m+n}, \\[4pt]
(10) & \left(t_1,\ 1,\ \underline{0},\ \hspace{5em} t_2\ \right) \quad \text{provided } 1+2\alpha-m-n=0 \text{ and } \lambda = \frac{-1-m}{1+m+n},
\end{array}
$$

$$
(11) \quad \left(-\frac{(\alpha-m-n)(1+m+n)}{(1+\alpha)(1+m)},\ \frac{2(\alpha-m-n)}{1+m}b,\ \frac{2(1+\alpha)}{1+2\alpha-m-n},\ \frac{1+m+n}{1+\alpha} - \frac{n(1+2\alpha-m-n)}{2(1+\alpha)^2}\right),
$$

$$
(12) \quad \left(\left(\frac{2\alpha(1+m)}{D(1-m-n)} + \frac{2(\alpha-m-n)}{D}\lambda\right)\left(\frac{2\alpha(1+m)}{D(1-m-n)} - \frac{1+m+n}{D}\lambda\right)\frac{1-m-n}{\lambda(2-n)}\frac{1-m-n}{\lambda(1+m)},\right.
$$

$$
\left.\left(\frac{2\alpha(1+m)}{D(1-m-n)} + \frac{2(\alpha-m-n)}{D}\lambda\right)\left(\frac{1+m}{D} + \frac{1+m+n}{D}\lambda\right)\frac{1-m-n}{\lambda(1+m)},\ \frac{2-n}{1-m-n},\ \underline{0}\right).
$$

The generic equilibria in $\mathscr{P}$ are M_0, M_1, (1), (3-4), (6), and (11 -12); the rest are valid for specific parameter values.

C The linearized problems around M_0 and M_1

The coefficient matrix for the linearized system (S) around the equlibrium M_0 is

$$
\begin{pmatrix}
2 & 0 & 0 & 0 \\
br_0 & 1 & 0 & 0 \\
\frac{r_0}{n}(\lambda r_0) & \frac{r_0}{n} & \frac{r_0}{n}\left(\frac{\alpha-m-n}{\lambda(1+\alpha)} - \frac{n\alpha}{\lambda(1+\alpha)r_0}\right) & \frac{r_0}{n}\left(\frac{\alpha r_0}{\lambda}\right) \\
s_0(\lambda r_0) & s_0 & s_0\left(\frac{\alpha-m-n}{\lambda(1+\alpha)} + \frac{n}{\lambda(1+\alpha)r_0}\right) & s_0\left(-\frac{r_0}{\lambda}\right)
\end{pmatrix}
=
\begin{pmatrix}
2 & 0 & 0 & 0 \\
br_0 & 1 & 0 & 0 \\
\frac{r_0}{n}(\lambda r_0) & \frac{r_0}{n} & \frac{r_0}{n}\frac{1}{\lambda}\left(1 - s_0 - \frac{n}{r_0}\right) & \frac{r_0}{n}\left(\frac{\alpha r_0}{\lambda}\right) \\
s_0(\lambda r_0) & s_0 & s_0\frac{1}{\lambda}(1 - s_0) & s_0\left(-\frac{r_0}{\lambda}\right)
\end{pmatrix}
$$

The corresponding eigenvectors X_{0j} are collected in the matrix S_0 as j-th column vector, $j = 1, 2, 3, 4$.

$$
S_0 = \begin{pmatrix}
1 & 0 & 0 & 0 \\
br_0 & 1 & 0 & 0 \\
y_1 & y_2 & 1 & y_4 \\
z_1 & z_2 & z_3 & 1
\end{pmatrix},
\qquad
\begin{pmatrix} y_1 \\ z_1 \end{pmatrix} = -(\lambda+b)r_0 \begin{pmatrix} \frac{\frac{1+\alpha}{\lambda}r_0+\frac{2}{s_0}}{\Delta_1} \\ \frac{\frac{n}{r_0}\left(\frac{1}{\lambda}+2\right)}{\Delta_1} \end{pmatrix},
\qquad
\begin{pmatrix} y_2 \\ z_2 \end{pmatrix} = -\begin{pmatrix} \frac{\frac{1+\alpha}{\lambda}r_0+\frac{\mu_{02}}{s_0}}{\Delta_2} \\ \frac{\frac{n}{r_0}\left(\frac{1}{\lambda}+\mu_{02}\right)}{\Delta_2} \end{pmatrix}
\tag{69}
$$

$$
z_3 = n\left(\frac{\frac{1-s_0}{\lambda}}{\frac{nr_0}{\lambda}+\frac{n\mu_0^+}{s_0}}\right), \qquad y_4 = \frac{\frac{r_0}{\lambda}+\frac{\mu_0^-}{s_0}}{\frac{1-s_0}{\lambda}},
$$

where $\Delta_1 = \frac{1-s_0}{\lambda}\left(\frac{1+\alpha}{\lambda}r_0 + \frac{2}{s_0}\right) - \frac{n}{r_0}\left(\frac{1}{\lambda} + 2\right)\left(\frac{r_0}{\lambda} + \frac{2}{s_0}\right)$ and $\Delta_2 = \frac{1-s_0}{\lambda}\left(\frac{1+\alpha}{\lambda}r_0 + \frac{1}{s_0}\right) - \frac{n}{r_0}\left(\frac{1}{\lambda} + 1\right)\left(\frac{r_0}{\lambda} + \frac{1}{s_0}\right)$.
We find that $y_1, y_2, y_4 < 0$; $z_1, z_2, z_3 \sim O(n)$, provided n is sufficiently small.

Next, the coefficient matrix for the linearized system around M_1 is

$$
\begin{pmatrix}
-\frac{1+m+n}{\alpha-m-n} & 0 & 0 & 0 \\
(b-\lambda)r_1 & -1 & 0 & 0 \\
\frac{r_1}{n}(\lambda r_1) & \frac{r_1}{n} & \frac{r_1}{n}\left(\frac{\alpha-m-n}{\lambda(1+\alpha)}-\frac{n\alpha}{\lambda(1+\alpha)r_1}\right) & \frac{r_1}{n}(\frac{\alpha r_1}{\lambda}) \\
s_1(\lambda r_1) & s_1 & s_1\left(\frac{\alpha-m-n}{\lambda(1+\alpha)}+\frac{n}{\lambda(1+\alpha)r_1}\right) & s_1(-\frac{r_1}{\lambda})
\end{pmatrix}
=
\begin{pmatrix}
-\frac{1+m+n}{\alpha-m-n} & 0 & 0 & 0 \\
(b-\lambda)r_1 & -1 & 0 & 0 \\
\frac{r_1}{n}(\lambda r_1) & \frac{r_1}{n} & \frac{r_1}{n}\frac{1}{\lambda}\left(1-s_1-\frac{n}{r_1}\right) & \frac{r_1}{n}(\frac{\alpha r_1}{\lambda}) \\
s_1(\lambda r_1) & s_1 & s_1\frac{1}{\lambda}(1-s_1) & s_1(-\frac{r_1}{\lambda})
\end{pmatrix}
$$

In what follows we examine all possible cases: Except for the case $\mu_{11}=\mu_{12}=-1$, four linearly independent eigenvectors are attained. In the exceptional case $\mu_{11}=\mu_{12}=-1$ the repeated eigenvalue -1 has geometric multiplicity which is strictly less that its algebraic multiplicity.

As to the eigenvectors, notice that the eigenvalues for M_1 (differently from those for M_0) have the chance to be repeated. The analysis below shows that, unless $\mu_{11}=\mu_{12}=-1$, four linearly independent eigenvectors are attained. If the exceptional case takes place then we will supplement precisely one generalized eigenvector for the repeated eigenvalue -1.

Case 1. $-\frac{1+m+n}{\alpha-m-n}\neq -1$; or $-\frac{1+m+n}{\alpha-m-n}=-1$ **but** $b=\lambda$. This case yields four linearly independent eigenvectors. The eigenvectors X_{1j} are collected in the matrix S_1 as j-th column vector, $j=1,2,3,4$, and in the case of repeated eigenvalues the corresponding eigenvectors are understood as a basis for the associated subspace:

$$
S_1=\begin{pmatrix}
1 & 0 & 0 & 0 \\
x_1 & 1 & 0 & 0 \\
y_1 & y_2 & 1 & y_4 \\
z_1 & z_2 & z_3 & 1
\end{pmatrix},
\qquad
x_1=\begin{cases}\frac{(b-\lambda)r_1}{1+\mu_{11}} & \text{if }\mu_{11}\neq -1,\\ 0 & \text{otherwise,}\end{cases}
$$

$$
z_3=n\left(\frac{\frac{1-s_1}{\lambda}}{\frac{nr_1}{\lambda}+\frac{n\mu_1^+}{s_1}}\right),\qquad y_4=\frac{\frac{r_1}{\lambda}+\frac{\mu_1^-}{s_1}}{\frac{1-s_1}{\lambda}},
$$

$$
\begin{pmatrix}y_1\\z_1\end{pmatrix}=
\begin{cases}
-(\lambda r_1+x_1)\begin{pmatrix}\frac{\lambda}{1-s_1}\\0\end{pmatrix} & \text{if }\mu_{14}=\mu_{11},\\[2ex]
-(\lambda r_1+x_1)\begin{pmatrix}\frac{\frac{1+\alpha}{\lambda}r_1+\frac{\mu_{11}}{s_1}}{\Delta_3}\\\frac{\frac{n}{r_1}\left(\frac{1}{\lambda}+\mu_{11}\right)}{\Delta_3}\end{pmatrix} & \text{otherwise,}
\end{cases}
\qquad
\begin{pmatrix}y_2\\z_2\end{pmatrix}=
\begin{cases}
-\begin{pmatrix}\frac{\lambda}{1-s_1}\\0\end{pmatrix} & \text{if }\mu_{14}=\mu_{12},\\[2ex]
-\begin{pmatrix}\frac{\frac{1+\alpha}{\lambda}r_1+\frac{\mu_{12}}{s_1}}{\Delta_4}\\\frac{\frac{n}{r_1}\left(\frac{1}{\lambda}+\mu_{12}\right)}{\Delta_4}\end{pmatrix} & \text{otherwise,}
\end{cases}
\tag{70}
$$

where

$$
\Delta_3=\frac{1-s_1}{\lambda}\left(\frac{1+\alpha}{\lambda}r_1+\frac{\mu_{11}}{s_1}\right)-\frac{n}{r_1}\left(\frac{1}{\lambda}+\mu_{11}\right)\left(\frac{r_1}{\lambda}+\frac{\mu_{11}}{s_1}\right)
$$
$$
=\frac{-n}{r_1 s_1}\det\left[\begin{pmatrix}\frac{r_1}{n}\left(\frac{1-s_1}{\lambda}-\frac{n}{\lambda r_1}\right) & \frac{r_1}{n}\frac{\alpha r_1}{\lambda}\\ s_1\frac{1-s_1}{\lambda} & -s_1\frac{r_1}{\lambda}\end{pmatrix}-\mu_{11}\mathrm{I}\right]\neq 0,
$$
$$
\Delta_4=\frac{1-s_1}{\lambda}\left(\frac{1+\alpha}{\lambda}r_1+\frac{\mu_{12}}{s_1}\right)-\frac{n}{r_1}\left(\frac{1}{\lambda}+\mu_{12}\right)\left(\frac{r_1}{\lambda}+\frac{\mu_{12}}{s_1}\right)
$$
$$
=\frac{-n}{r_1 s_1}\det\left[\begin{pmatrix}\frac{r_1}{n}\left(\frac{1-s_1}{\lambda}-\frac{n}{\lambda r_1}\right) & \frac{r_1}{n}\frac{\alpha r_1}{\lambda}\\ s_1\frac{1-s_1}{\lambda} & -s_1\frac{r_1}{\lambda}\end{pmatrix}-\mu_{12}\mathrm{I}\right]\neq 0
$$

respectively for the corresponding cases.

Case 2. $-\frac{1+m+n}{\alpha-m-n}=-1$ **and** $b\neq\lambda$: For this case $\mu_{11}=\mu_{12}=-1$ has algebraic multiplicity two but its geometric multiplicity is one, so we replace the first column of S_1 by the generalized eigenvector $\left(\frac{1}{(b-\lambda)r_1},0,y_1',z_1'\right)^T$, where

$$
\begin{pmatrix}y_1'\\z_1'\end{pmatrix}=
\begin{cases}
\begin{pmatrix}-\frac{\lambda}{1-s_1}\left(\frac{\lambda}{b-\lambda}-\frac{n}{r_1}z_2\right)\\0\end{pmatrix} & \text{if }\mu_{14}=-1,\\[3ex]
-\frac{\lambda}{b-\lambda}\begin{pmatrix}\frac{\frac{1+\alpha}{\lambda}r_1+\frac{\mu_{11}}{s_1}}{\Delta_3}\\\frac{\frac{n}{r_1}\left(\frac{1}{\lambda}+\mu_{11}\right)}{\Delta_3}\end{pmatrix}+\frac{n}{r_1}\begin{pmatrix}\frac{y_2\left(\frac{r_1}{\lambda}+\frac{\mu_{11}}{s_1}\right)+z_2\frac{\alpha r_1}{\lambda}}{\Delta_3}\\\frac{y_2\left(\frac{1-s_1}{\lambda}\right)+z_2\left(-\frac{1-s_1}{\lambda}+\frac{n}{r_1}\left(\frac{1}{\lambda}+\mu_{11}\right)\right)}{\Delta_3}\end{pmatrix} & \text{otherwise.}
\end{cases}
\tag{71}
$$

34

$$0 = Mat_1 \begin{pmatrix} w \\ x \\ y \\ z \end{pmatrix} - \mu \begin{pmatrix} w \\ x \\ y \\ z \end{pmatrix} = \begin{pmatrix} (\mu_{11} - \mu)w \\ (b-\lambda)r_1 w + (\mu_{12} - \mu)x \\ \frac{r_1}{n}\left[\lambda r_1 w + x + \left(\frac{1-s_1}{\lambda} - \frac{n}{r_1}\left(\frac{1}{\lambda} + \mu\right)\right)y + \frac{\alpha r_1}{\lambda}z\right] \\ s_1\left[\lambda r_1 w + x + \left(\frac{1-s_1}{\lambda}\right)y - \left(\frac{r_1}{\lambda} + \frac{\mu}{s_1}\right)z\right] \end{pmatrix},$$

$$A \triangleq \begin{pmatrix} \frac{1-s_1}{\lambda} - \frac{n}{r_1}\left(\frac{1}{\lambda} + \mu\right) & \frac{\alpha r_1}{\lambda} \\ \frac{1-s_1}{\lambda} & -\left(\frac{r_1}{\lambda} + \frac{\mu}{s_1}\right) \end{pmatrix} \begin{pmatrix} y \\ z \end{pmatrix} = -(\lambda r_1 w + x)\begin{pmatrix} 1 \\ 1 \end{pmatrix}$$

$$A^{-1} = \frac{1}{\Delta}\begin{pmatrix} \left(\frac{r_1}{\lambda} + \frac{\mu}{s_1}\right) & \frac{\alpha r_1}{\lambda} \\ \frac{1-s_1}{\lambda} & -\frac{1-s_1}{\lambda} + \frac{n}{r_1}\left(\frac{1}{\lambda} + \mu\right) \end{pmatrix}, \quad \Delta = \frac{1-s_1}{\lambda}\left(\frac{1+\alpha}{\lambda}r_1 + \frac{\mu}{s_1}\right) - \frac{n}{r_1}\left(\frac{1}{\lambda} + \mu\right)\left(\frac{r_1}{\lambda} + \frac{\mu}{s_1}\right)$$

References

[1] M. BERTSCH, L. PELETIER, AND S. VERDUYN LUNEL, The effect of temperature dependent viscosity on shear flow of incompressible fluids, *SIAM J. Math. Anal.* **22** (1991), 328–343.

[2] R.J. CLIFTON, High strain rate behaviour of metals, *Appl. Mech. Rev.* **43** (1990), S9-S22.

[3] R.J.CLIFTON, J.DUFFY, K.A.HARTLEY AND T.G.SHAWKI, On critical conditions for shear band formation at high strain rates, *Scripta Met.*, **18** (1984), pp. 443-448.

[4] L.S.COSTIN, E.E.CRISMAN, R.H.HAWLEY, AND J.DUFFY, *On the localization of plastic flow in mild steel tubes under dynamic torsional loading* In "Proc. 2nd Conf. on the Mechanical Properties of Materials at high rates of strain", Inst. Phys. Conf. Ser. no 47, Oxford, 90, 1979.

[5] C.M. DAFERMOS AND L. HSIAO, Adiabatic shearing of incompressible fluids with temperature-dependent viscosity. *Quart. Applied Math.* **41** (1983), 45–58.

[6] E.J. DOEDEL, AUTO: A program for the automatic bifurcation analysis of autonomous systems, *Cong. Numer.* **30** (1981), 265–284.

[7] E.J. DOEDEL AND J.P. KERNEVEZ, AUTO: Software for continuation and bifurcation problems in ordinary differential equations, Applied Mathematics Report, California Institute of Technology, (1986), 226 pages.

[8] E.J. DOEDEL, A.R. CHAMPNEYS, T.F. FAIRGRIEVE, Y.A. KUZNETSOV, B. SANDSTEDE, AND X. WANG, AUTO 97: Continuation And Bifurcation Software For Ordinary Differential Equations (with HomCont), (1999), (http://indy.cs.concordia.ca/auto/)

[9] N. FENICHEL, Persistence and smoothness of invariant manifolds for flows, *Indiana Univ. Math. J.* **21** (1972) 193–226.

[10] N. FENICHEL, Asymptotic stability with rate conditions, *Indiana Univ. Math. J.* **23** (1974) 1109–1137.

[11] N. FENICHEL, Asymptotic stability with rate conditions II, *Indiana Univ. Math. J.* **26** (1977) 81–93.

[12] N. FENICHEL, Geometric singular perturbation theory for ordinary differential equations, *J. Differ. Equations* **31** (1979), 53–98.

[13] C. Fressengeas and A. Molinari Instability and localization of plastic flow in shear at high strain rates, *J Mech Phys Solids* **35** (1987), pp. 185-211.

[14] K.A.Hartley, J.Duffy, and R.J.Hawley, Measurement of the temperature profile during shear band formation in steels deforming at high-strain rates *J. Mech. Physics Solids*, **35** (1987), 283-301.

[15] J.W. Hutchinson and K.W. Neale, Influence of strain-rate sensitivity on necking under uniaxial tension, *Acta Metallurgica* **25** (1977), 839-846.

[16] Th. Katsaounis, J. Olivier, and A.E. Tzavaras, Emergence of coherent localized structures in shear deformations of temperature dependent fluids, *Archive for Rational Mechanics and Analysis* **224** (2017), 173–208.

[17] Th. Katsaounis and A.E. Tzavaras, Effective equations for localization and shear band formation, *SIAM J. Appl. Math.* **69** (2009), 1618–1643.

[18] Th. Katsaounis, M.-G. Lee, and A.E. Tzavaras, Localization in inelastic rate dependent shearing deformations, *J. Mech. Phys. of Solids* **98** (2017), 106–125.

[19] M.-G. Lee, Th. Katsaounis, and A.E. Tzavaras, Localization of Adiabatic Deformations in Thermoviscoplastic Materials, In Proceedings of the 16th International Conference on Hyperbolic Problems: Theory, Numerics, Applications (HYP2016), to appear.

[20] C. K. R. T. Jones, Geometric singular perturbation theory. Dynamical systems (Montecatini Terme, 1994), pp 44118, *Lecture Notes in Math.*, 1609, Springer, Berlin, 1995.

[21] C. Kuehn, *Multiple time scale dynamics*, Applied Mathematical Sciences, Vol. **191** (Springer Basel 2015).

[22] M.-G. Lee and A.E. Tzavaras, Existence of localizing solutions in plasticity via the geometric singular perturbation theory, *Siam J. Appl. Dyn. Systems* **16** (2017), 337–360.

[23] A.Molinari and R.J.Clifton, *Analytical characterization of shear localization in thermoviscoplastic materials* J. Appl. Mech., **54** (1987), 806-812.

[24] T.G. Shawki and R.J. Clifton, Shear band formation in thermal viscoplastic materials, *Mech. Mater.* **8** (1989), 13–43.

[25] P. Szmolyan, Transversal heteroclinic and homoclinic orbits in singular perturbation problems, *J. Differ. Equations* **92** (1991), 252–281.

[26] A.E. Tzavaras, Shearing of materials exhibiting thermal softening or temperature dependent viscosity, *Quart. Applied Math.* **44** (1986), 1–12.

[27] A.E. Tzavaras, Effect of thermal softening in shearing of strain-rate dependent materials. *Archive for Rational Mechanics and Analysis*, **99** (1987), 349–374.

[28] A.E. Tzavaras, Plastic shearing of materials exhibiting strain hardening or strain softening, *Arch. Ration. Mech. Anal.* **94** (1986), 39–58.

[29] A.E. Tzavaras, Nonlinear analysis techniques for shear band formation at high strain-rates, *Appl. Mech. Rev.* **45** (1992), S82–S94.

[30] T.W. Wright, *The Physics and Mathematics of Shear Bands.* (Cambridge Univ. Press 2002).

[31] C. Zener and J. H. Hollomon, Effect of strain rate upon plastic flow of steel, *J. Appl. Phys.* **15** (1944), 22–32.